NAVAL POSTGRADUATE SCHOOL
Monterey, California

(2)

THESIS

COMPUTER SIMULATION OF ACOUSTIC FLUCTUATIONS DUE TO FINESCALE TEMPERATURE PERTURBATIONS MEASURED BY THERMISTOR CHAIN

by

Gregory D. Crabtree

March1992

Thesis Advisor: Pecheng Chu

Approved for public release; distribution is unlimited.

REPORT DOCUMENTATION PAGE

1a. REPORT SECURITY CLASSIFICATION: UNCLASSIFIED	1b. RESTRICTIVE MARKINGS
2a. SECURITY CLASSIFICATION AUTHORITY	3. DISTRIBUTION/AVAILABILITY OF REPORT: Approved for public release; distribution is unlimited
2b. DECLASSIFICATION/DOWNGRADING SCHEDULE	
4. PERFORMING ORGANIZATION REPORT NUMBER(S)	5. MONITORING ORGANIZATION REPORT NUMBER(S)
6a. NAME OF PERFORMING ORGANIZATION: Oceanography Dept. Naval Postgraduate School; 6b. OFFICE SYMBOL (if applicable): OC	7a. NAME OF MONITORING ORGANIZATION: Naval Postgraduate School
6c. ADDRESS (City, State, and ZIP Code): Monterey, CA 93943-5000	7b. ADDRESS (City, State, and ZIP Code): Monterey, CA 93943-5000
8a. NAME OF FUNDING/SPONSORING ORGANIZATION; 8b. OFFICE SYMBOL (if applicable)	9. PROCUREMENT INSTRUMENT IDENTIFICATION NUMBER
8c. ADDRESS (City, State, and ZIP Code)	10. SOURCE OF FUNDING NUMBERS: PROGRAM ELEMENT NO. / PROJECT NO. / TASK NO. / WORK UNIT ACCESSION NO.

11. TITLE (Include Security Classification)
COMPUTER SIMULATION OF ACOUSTIC FLUCTUATIONS DUE TO FINESCALE TEMPERATURE PERTURBATIONS MEASURED BY THERMISTOR CHAIN (U)

12. PERSONAL AUTHOR(S)
Crabtree, Gregory D.

13a. TYPE OF REPORT	13b. TIME COVERED	14. DATE OF REPORT (Year, Month, Day)	15. PAGE COUNT
Master's Thesis	FROM 05/89 TO 03/90	March 1992	56

16. SUPPLEMENTARY NOTATION: The views expressed in this thesis are those of the author and do not reflect the official policy or position of the Department of Defense or the United States Government.

17. COSATI CODES			18. SUBJECT TERMS (Continue on reverse if necessary and identify by block number)
FIELD	GROUP	SUB-GROUP	Acoustic fluctuations, finescale, surface duct, temperature perturbations, parabolic equation, Kolmogorov spectra

19. ABSTRACT (Continue on reverse if necessary and identify by block number)

Finescale temperature features in the oceanic mixed layer (OML) modify acoustic propagation by perturbing the index of refraction. A thermistor chain measures temperature from the surface to 250 m with 2 m vertical resolution and 1.85 m horizontal resolution. Thermistor data is converted to high resolution sound velocity profiles for input to an implicit finite difference parabolic equation (IFD-PE) model. The control case is a surface duct with a horizontally averaged sound velocity profile. The IFD-PE model is run with monofrequency sources from 500 Hz to 10 kHz. The acoustic fluctuations and average acoustic pressure are computed each 20 km to a range of 100 km. Acoustic propagation through the temperature varying OML is contrasted with acoustic propagation through the temperature invariant OML. Finescale temperature randomly alters the average acoustic pressure by up to a factor of two and the acoustic fluctuations by up to a factor of five.

20. DISTRIBUTION/AVAILABILITY OF ABSTRACT: [X] UNCLASSIFIED/UNLIMITED [ ] SAME AS RPT. [ ] DTIC USERS	21. ABSTRACT SECURITY CLASSIFICATION: UNCLASSIFIED
22a. NAME OF RESPONSIBLE INDIVIDUAL: Pecheng Chu	22b. TELEPHONE (Include Area Code): (408) 646-3257; 22c. OFFICE SYMBOL: OC/Cu

DD FORM 1473, 84 MAR — 83 APR edition may be used until exhausted. All other editions are obsolete.

Approved for public release; distribution is unlimited

COMPUTER SIMULATION OF ACOUSTIC FLUCTUATIONS DUE TO FINESCALE TEMPERATURE PERTURBATIONS MEASURED BY THERMISTOR CHAIN

by
Gregory D. Crabtree
Lieutenant, United States Navy
B.S., United States Naval Academy, 1984

Submitted in partial fulfillment of the
requirements for the degree of

MASTER OF SCIENCE IN PHYSICAL OCEANOGRAPHY

from the

NAVAL POSTGRADUATE SCHOOL
MARCH 1992

Author: _____
Gregory D. Crabtree

Approved By: _____
Pecheng Chu, Thesis Advisor

_____
Anthony A. Atchley, Second Reader

_____
Curtis A. Collins, Chairman,
Department of Oceanography

ABSTRACT

Finescale temperature features in the oceanic mixed layer (OML) modify acoustic propagation by perturbing the index of refraction. A thermistor chain measures temperature from the surface to 250 m with 2 m vertical resolution and 1.85 m horizontal resolution. Thermistor data is converted to high resolution sound velocity profiles for input to an implicit finite difference parabolic equation (IFD-PE) model. The control case is a surface duct with a horizontally averaged sound velocity profile. The IFD-PE model is run with monofrequency sources from 500 Hz to 10 kHz. The acoustic fluctuations and average acoustic pressure are computed each 20 km to a range of 100 km. Acoustic propagation through the temperature varying OML is contrasted with acoustic propagation through the temperature invariant OML. Finescale temperature randomly alters the average acoustic pressure by up to a factor of two and the acoustic fluctuations by up to a factor of five.

TABLE OF CONTENTS

I. INTRODUCTION 1
A. SCALES OF MEDIA SOUND SPEED PERTURBATIONS 1
B. PREVIOUS WORK 2

II. THERMISTOR CHAIN DATA 5
A. DESCRIPTION OF NEAT GIN DATA COLLECTION 5
B. DESCRIPTION OF THE MIXED LAYER IN GENERAL 5
C. THERMISTOR CHAIN DATA SET 6
1. Statistical Analysis of Thermistor Chain Data 8
a. Horizontally Averaged Temperature Profile 8
b. Standard Deviation of Temperature Versus Depth 9
c. Temperature Density Spectra at Selected Depths 10

III. ACOUSTIC PROPAGATION IN INHOMOGENEOUS WATER 12
A. WAVE EQUATION IN INHOMOGENEOUS OCEAN 12
B. PARABOLIC WAVE EQUATION 15

IV. ACOUSTIC SIMULATION 17
A. ASSUMPTIONS IN THE COMPUTER SIMULATION 18
1. Temporally Frozen 18
2. Artificial Absorbing Bottom 18
3. Gaussian Starting Field 19
4. Isohaline 19
5. Other Scatterers 20
B. STATISTICS OF ACOUSTIC PROPAGATION THROUGH OML 20

V. DISCUSSION OF RESULTS 36
A. Range Dependence of Acoustic Propagation in a Surface Duct 36
B. Frequency Dependence of Acoustic Propagation through a Surface Duct 38
C. Dependence of Acoustic Propagation on Finescale Temperature Perturbations 39
D. Dependence of Acoustic Propagation on Source Depth 40

VI. CONCLUSIONS 48
A. HIGHLIGHTS 48
B. SUGGESTIONS FOR FURTHER WORK 48

REFERENCES 49

INITIAL DISTRIBUTION LIST 50

I. INTRODUCTION

Most acoustic predictions are based on strong assumptions about the oceanic mixed layer (OML) which are accurate only to a first degree. One assumption is OML depth does not have horizontal variation. In fact, internal waves propagate along the OML-thermocline interface and change its depth by typically 5-10m. Another assumption is the OML is both isohaline and isothermal, leading to a deterministic sound speed profile with variation in depth dependent only on pressure. In reality, as cool underlying water is mixed upward and warm surface water is mixed downward, there is temperature variation throughout the OML. The temperature variance causes corresponding variance in the sound speed profile. The objective of this work is to determine how good these assumptions are for medium frequencies propagating long distances.

A thermistor chain data set collected in October 1989 in the Norwegian Current system is discussed and analyzed in Chapter II. Thermistor chain data provides a two dimensional profile from the surface down to 250 m with 2 m resolution in the vertical and 1.85 m resolution in the horizontal. The data is converted to a series of high resolution sound velocity profiles with spacing at every 1.85 m in the horizontal. These profiles are the input for a computer simulation of acoustic transmission. Chapter III discusses acoustic transmission through a temperature varying OML.

The Implicit Finite Difference Parabolic Equation (IFD-PE) acoustic model developed by Lee and McDaniel (1987) is modified to allow horizontal variation at the same distances as the thermistor chain data set was read. The IFD-PE acoustic model was run at several frequencies from 500 Hz to 10 kHz. Two simulations were run at each frequency: one with a realistic OML and the other with an idealized OML. In the realistic case the sound velocity profile is read into the acoustic model every 1.85 m. In the idealized case the temperature is averaged horizontally, yielding a single sound velocity profile for the entire event. The transmission loss with range for the two cases is computed at each frequency. Average acoustic pressure and the spatial variance of acoustic pressure are shown in Chapter IV. The difference between sound propagation through a real OML and through an idealized OML is discussed in Chapter V.

A. SCALES OF MEDIA SOUND SPEED PERTURBATIONS

The speed of sound in the ocean is a function of three parameters; temperature, salinity, and pressure. An increase in any one of these three quantities causes a corresponding increase in the speed of sound. The speed of sound in sea water used in this paper is that determined by Mackenzie (1981)

$$c(z) = 1448.96 + 4.591\,T - 5.304 \times 10^{-2}\,T^2 + 2.374 \times 10^{-4}\,T^3$$
$$+1.340\,(S-35) + 1.630 \times 10^{-2}\,z + 1.675 \times 10^{-7}\,z^2 \qquad (1.1)$$
$$-1.025 \times 10^{-2}\,T\,(S-35) - 7.139 \times 10^{-13}\,T\,z^3$$

where T is temperature in °C, S is salinity in practical salinity units, and z is depth in meters. Pressure effect depends almost exclusively on depth in the water column and pressure effects due to dynamic motions are not considered.

The integral scale of convective mixing in the mixed layer is approximately the depth of the OML. Overturning water is an unstable process which creates turbulence. There is a cascade of energy from the integral scale down to 1 cycle per meter (cpm) as large vortices dissipate into increasingly smaller vortices. Dissipation dominates at distances less than this, causing the cascade of temperature density spectra to decay less rapidly (Flatté, 1979, p. 15). The region between 1 m and 100 m is finestructure scale and is the regime within the purview of this paper.

Individual finestructure features in the ocean are large enough to be accurately measured with modern instruments, but too small and too brief to be included in ocean basin models and nowcasts. Rather than model isolated features independently it is more practical to describe them by wavenumber spectra. Temperature perturbations collected in this thermistor chain data set are for this reason converted to temperature variance spectra. The wavenumber spectra of temperature variance for this analysis range between 0.27 m^{-1} (1 cycle every 3.7 m) and 0.004 m^{-1} (1 cycle every 237 m).

B. PREVIOUS WORK

Underwater sound propagation has been studied in earnest ever since World War II. The earliest transmission loss models were horizontally homogeneous. They relied on a single sound velocity profile (SVP) assumed to be the same at all locations. These models were unable to accurately predict transmission loss across fronts and eddies. Models based on ray theory and (later) the parabolic equation approximation enabled acousticians to model range dependent transmission loss. Range independent and range dependent models have been relied upon to provide the general features of transmission loss predictions right up to the present with excellent accuracy. Their drawback is they model a deterministic transmission path through a very non-deterministic medium. Because of the effects of constructive and destructive interference from multipath arrivals, slight variations in sound speed have a large influence on the actual ranges of the features of transmission loss curves. For this reason acoustic propagation is best characterized statistically for most applications.

An emphasis on the statistics of acoustic propagation has generated considerable theoretical and experimental activity. Theoretical treatments have their roots in scattering theory first pioneered by Rytov (1937). He addressed scattering by small perturbations of a media valid for electromagnetic propagation through the atmosphere as well as for acoustic propagation. Chernov (1960) considered the case of isotropic perturbations by using the method of small perturbations and applying an autocorrelation distance to the inhomogeneities. His derivation relied on a single temperature correlation coefficient rather than on a temperature spectra. Tatarskii (1961) included a spectrum of scales of processes. Neither he nor Chernov specialized to ocean processes and they assumed media perturbations to be isotropic. In reality almost all ocean features greater than 1 m in length are anisotropic, varying much more in the vertical than in the horizontal (Flatté, 1979, p. 15).

Most of the recent work on acoustic scattering by random media has specialized to scattering by internal waves in the deep sound channel. Highlights are Munk and Zachariason (1976) who used the Rytov method (also called supereikonal method) with a gaussian distribution of sound speed perturbations to address this problem. They assumed the internal wave spectrum presented by Garrett and Munk (1975) for the ocean medium. Flatté, et al (1979) also started with the Garrett - Munk internal wave model and presented alternative acoustic models to describe acoustic fluctuations statistically. Using ray theory, Ko (1981) passed multiple rays through a time stepped internal wave model within a deep sound channel. He used the Monte Carlo method to determine the statistics of acoustic wave propagation.

Although most of the effort in this field has been expended on propagation through the deep sound channel, there has been an increased interest on scattering of acoustic energy by finestructure scale perturbations. Wilson and Tappert (1979) model surface duct losses due to scattering by random fluctuations and below duct ensonification by radiation transport (i.e. energy flux). Duda, et al (1988) used computed spectra of sound speed fluctuations due to microstructure and fine structure to determine the variance and the wave number spectra of acoustic intensity. They investigated only the region with small fresnel radius and valid for the Rytov approximation which indicates that the frequency is less than 90 kHz and the range is less than 1.1 km. Furthermore, they considered only a single direct path propagation mode.

Like many contributions to this field, this thesis research is based on a computer simulation of acoustic propagation to determine the statistics of the propagation. It is unique, however, because it does not rely on theoretical model spectra of ocean features. It uses real temperature data. The combination of an extremely accurate acoustic model and high resolution real data provides a way to directly compare acoustic propagation in a real world horizontally varying OML to that of an idealized horizontally homogeneous OML, albeit with

some simplifying assumptions. These assumptions are described in chapter IV. The qualitative results are valid only for the particular temperature perturbation distribution and simplifying assumptions of this simulation. However, they provide insight into the magnitude of the effects of weak scattering by finestructure spectra within any surface duct.

II. THERMISTOR CHAIN DATA

A. DESCRIPTION OF NEAT GIN DATA COLLECTION

The thermistor chain data set that this computer simulation is based upon comes from the NEAT GIN ocean measurement trial. NEAT GIN data was collected by Dr. John Scott of the United Kingdom Admiralty Research Establishment in Fall of 1989. The data set selected was obtained in the Norwegian Current system on 11 October. It was collected from 1200 to 1800 GMT. The ship steamed at a nominally constant 4 knots and sampled thermistors every 1.9 seconds (1.852 m) for a total of 24,000 temperature soundings. The data set traverses a 44.5 km straight track. Thermistors were mounted every 2 m from the surface down to 250 m. This data set provides an extremely high resolution two dimensional temperature field.

B. DESCRIPTION OF THE MIXED LAYER IN GENERAL

Turbulent mixing forces the OML to be almost isothermal. Away from polar regions, temperature below the OML typically decreases with depth. Sound speed has a maximum at the base of the OML. Acoustic energy refracts away from the depth of the maximum sound speed. It is bent either upward into the duct or downward into the deep ocean. The ray bundles that refract upward are reflected from the ocean surface and continue to propagate within the OML. Since the OML traps sound, it is also called a surface duct. The depth of the surface duct is almost always the same as the depth of the OML.

The OML depth and temperature vary both temporally and spatially. Figure 1 shows oscillatory features in the thermocline right below the OML. These are caused by internal waves. Another characteristic of the OML apparent from this figure is the size of the largest temperature features. They vary vertically from 10 m to the depth of the OML and vary horizontally from 1 km to 5 km. Figure 2 makes the anisotropy of temperature features in the OML even more apparent. In this figure a small segment of the thermistor chain data is enlarged to show details. Two kilometers of the thermistor chain data is displayed in Fig 2a). The first 180 m of the same 2 km segment is shown in Fig 2b). They exhibit the anisotropy of larger features and the near isotropy of the near microstructure scale features. Contours greater than 40 m in depth traverse over 1 km horizontally. Those contours smaller than 5 m in depth traverse less than 10 m horizontally.

Aside from horizontal currents, most of the kinetic energy in the world oceans is contained in waves. This is true everywhere except very near the surface in the OML. Here turbulence dominates, and motions are regular in neither time nor space. Figures 1 and 2 depict the randomness of turbulent kinetic energy (TKE) in the OML.

C. THERMISTOR CHAIN DATA SET

Shown below is a contour plot of temperature from the 11 October 1989 thermistor chain data collection. It shows only the top 80 m of the entire 44.5 km track. The tightly spaced contours at the bottom

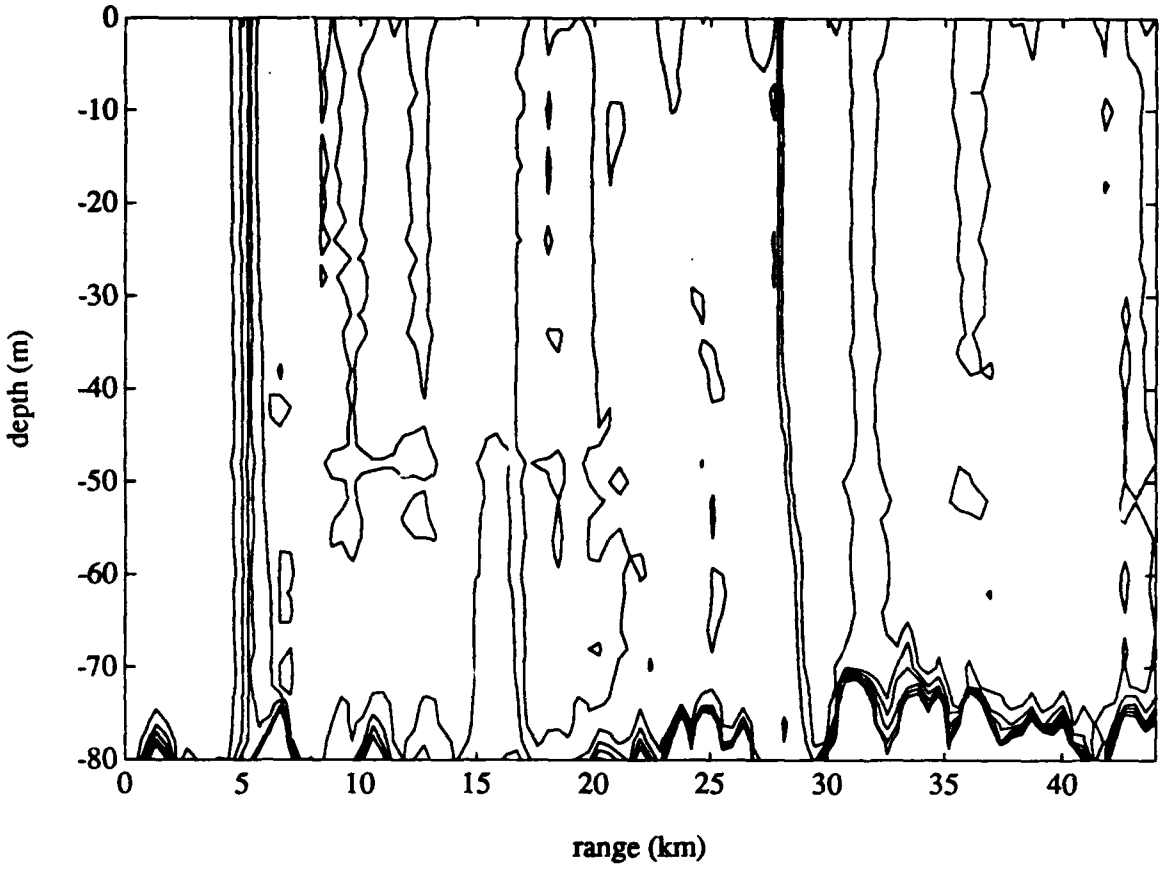

Fig 1. The upper ocean isotherms plotted from 7.9 °C to 8.2 °C with .05 °C increments.

of the plot indicate internal wave motions. They vary the OML depth between 70 m and 83 m. Temperature throughout the OML ranges 0.2 deg from 8.0 °C to 8.2 °C.

Selection of the 11 October 1989 data set was not based on significant features or characteristics contained in the data. Rather, it is suitable because it is typical of mid and high latitude conditions through much of the year. The OML depth remains relatively constant and temperature perturbations are mild. Modification of acoustic propagation by temperature perturbations in this sound channel is indicative of propagation through any surface duct.

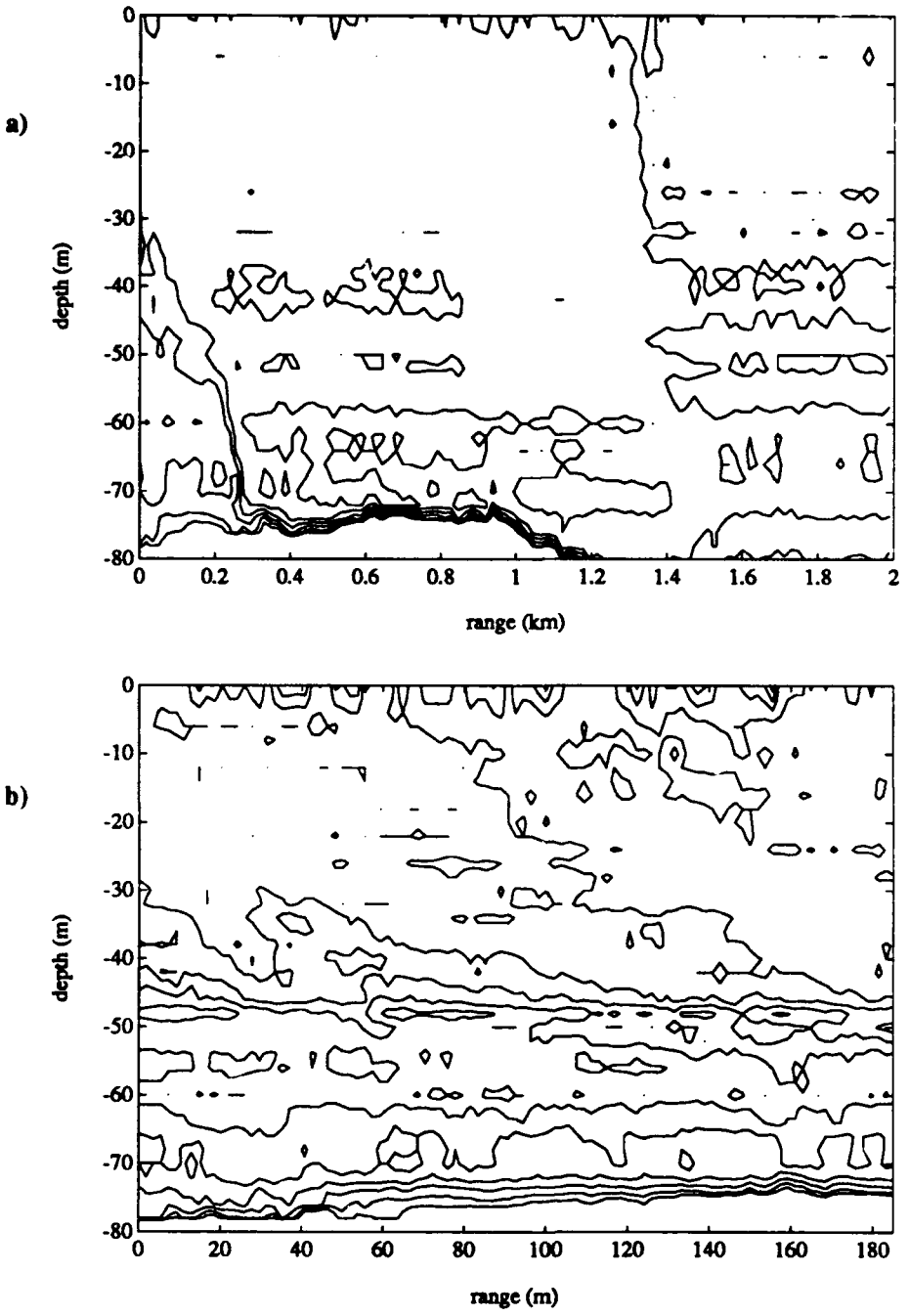

Fig 2. Sample of temperature features within the OML occurring over a) 2 km (varying from 8.0 to 8.14 °C with .02 °C increments) and b) 185 m (varying from 8.0 to 8.12 °C with .01 °C increments).

1. Statistical Analysis of Thermistor Chain Data

a. Horizontally Averaged Temperature Profile

Most acoustic transmission predictions assume an idealized sound velocity profile based on a single temperature sounding. They assume horizontal homogeneity based on a bathythermograph or climatological data. This thermistor chain data enables comparison of acoustic transmission through a real OML and through an idealized OML. The control case is an idealized OML generated by averaging thermistor chain values.

The horizontally averaged temperature profile for the thermistor chain data collected on October 11, 1989 is shown in Fig 3. Temperature perturbations are averaged out, leaving a near isothermal

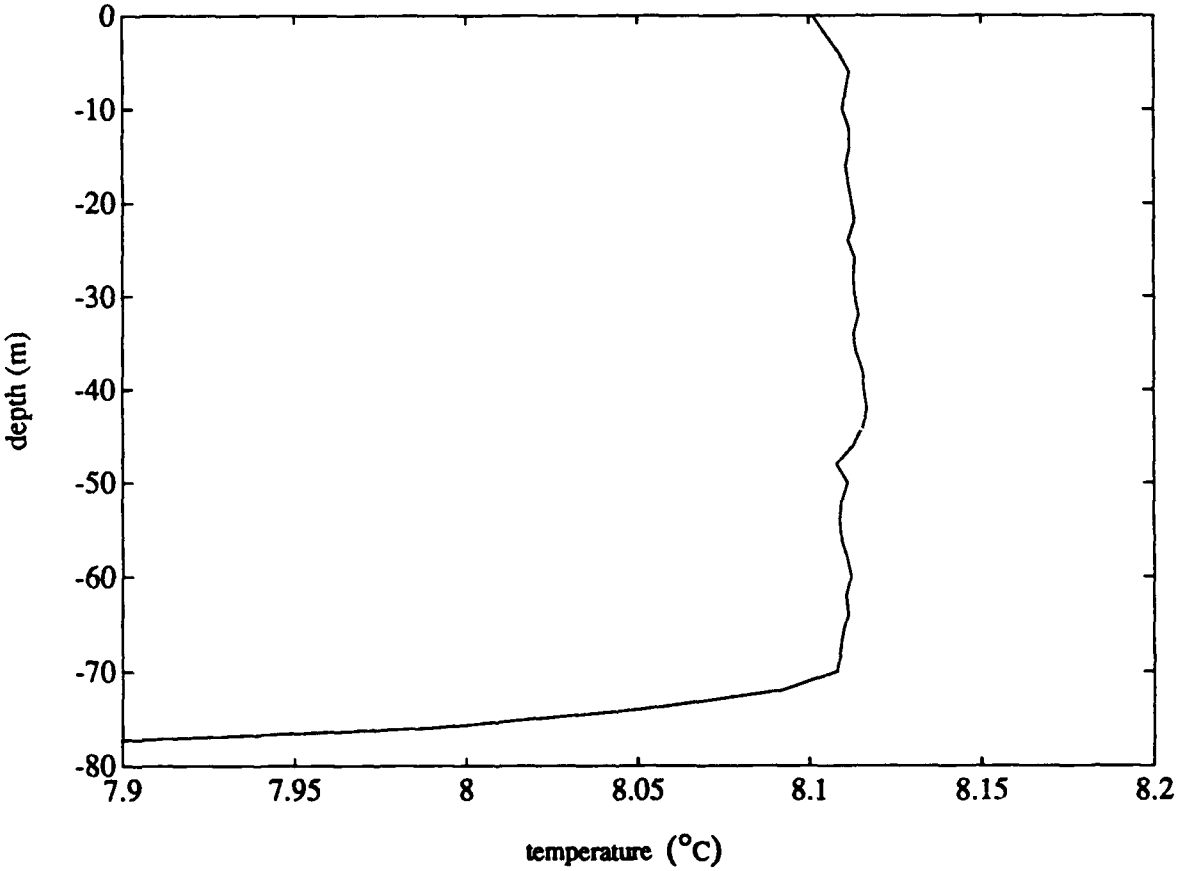

Fig 3. Horizontally averaged thermistor chain data set. All 24,000 profiles are averaged together at each of the 74 depths sampled. Only the top 80 m is shown.

OML of 8.1 °C. The kink defining the depth of the idealized OML is at 70 m. Below the OML is a thermocline that continues past the 250 m sampled depth. The gradient at the top of the thermocline is -.05 °C/m.

b. Standard Deviation of Temperature Versus Depth

The standard deviation of temperature from a horizontal mean is shown in Fig 4. This figure

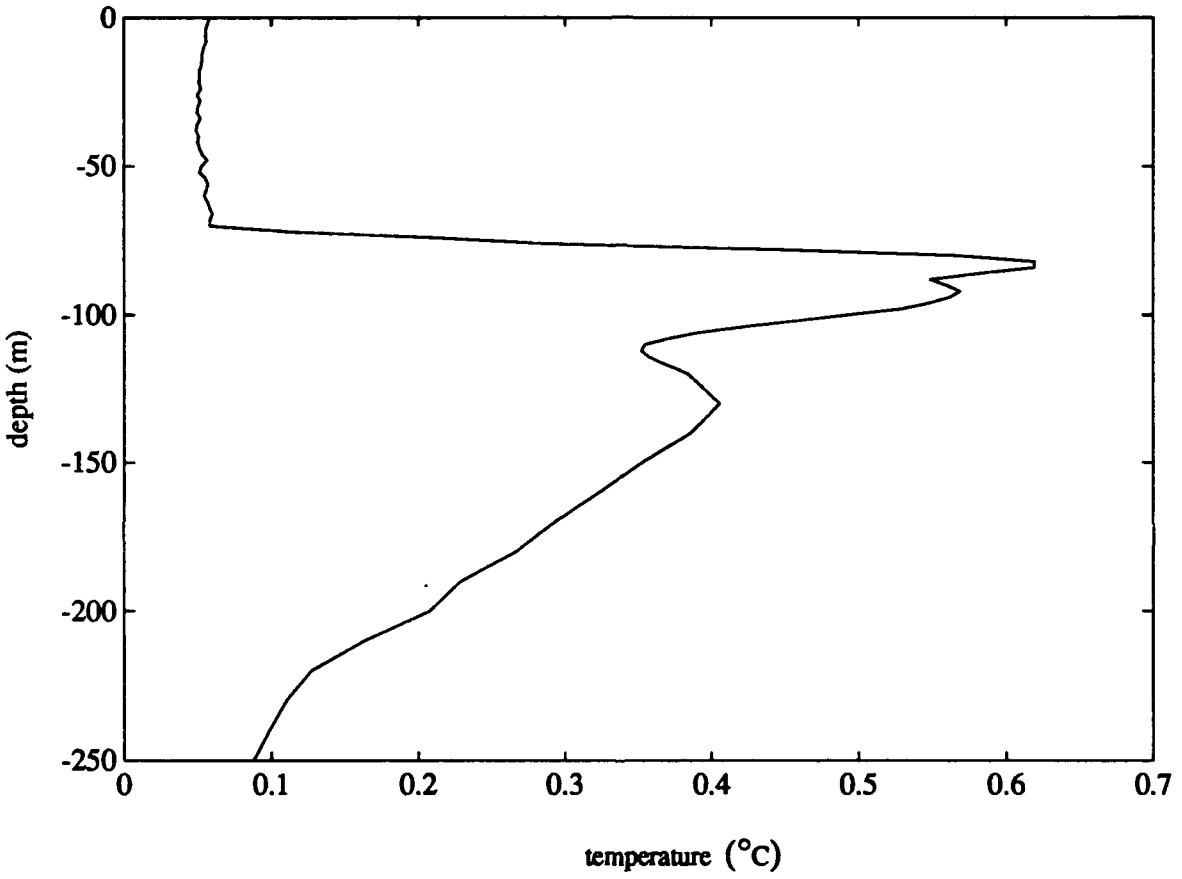

Fig 4. Depth dependence of standard deviation of temperature.

shows the standard deviation of temperature in the OML to be about 0.05 °C. It jumps dramatically below the OML because of internal waves propagating along the OML-thermocline interface. The discontinuity at 70 m highlights the OML depth. Temperature perturbations above this depth are characterized by small deviations generated by turbulent motions. The discontinuity at the depth of the OML is slightly misleading.

The large temperature variance occurs because the thermocline is lifted and lowered across this depth. Horizontal temperature changes in this region are quite gradual because the thermocline is stratified.

c. Temperature Density Spectra at Selected Depths

Temperature in the OML acts as a passive contaminant which closely follows turbulent velocity behavior (Medwin, 1973, p. 9). The Kolmogorov hypothesis states that fully developed turbulent velocity spectra depend only on kinematic shear viscosity ν and the rate of dissipation of energy ε. The velocity spectra and by inference the temperature spectra $\Phi(k)$ have been shown (Batchelor, 1956) to be related to the wavenumber of perturbations by

$$\Phi(k) = c_1 k^{-5/3}$$

where $c_1 = c_1(\nu, \varepsilon)$ is a constant at each depth. The Kolmogorov relationship is valid for the inertial subregion. The temperature spectra computed at various depths for the thermistor chain data are shown in Fig 5. Samples are each 237 m long, making the lowest resolvable wavenumber 0.004 m^{-1}. The Nyquist wavenumber is 0.27 m^{-1}. The temperature spectra fall within the inertial subregion for which the Kolmogorov relationship is valid. A solid line shows the theoretical $-\frac{5}{3}$ power law. At all three depths temperature variance is weighted primarily to the large scales and decays by an inverse power law to smaller scales. There are no statistically significant peaks within this data that would indicate regularly varying phenomena. As expected, most of the temperature variance in internal waves is associated with the largest scales. Temperature spectra in the OML mimic temperature spectra in the thermocline, but with much less variance.

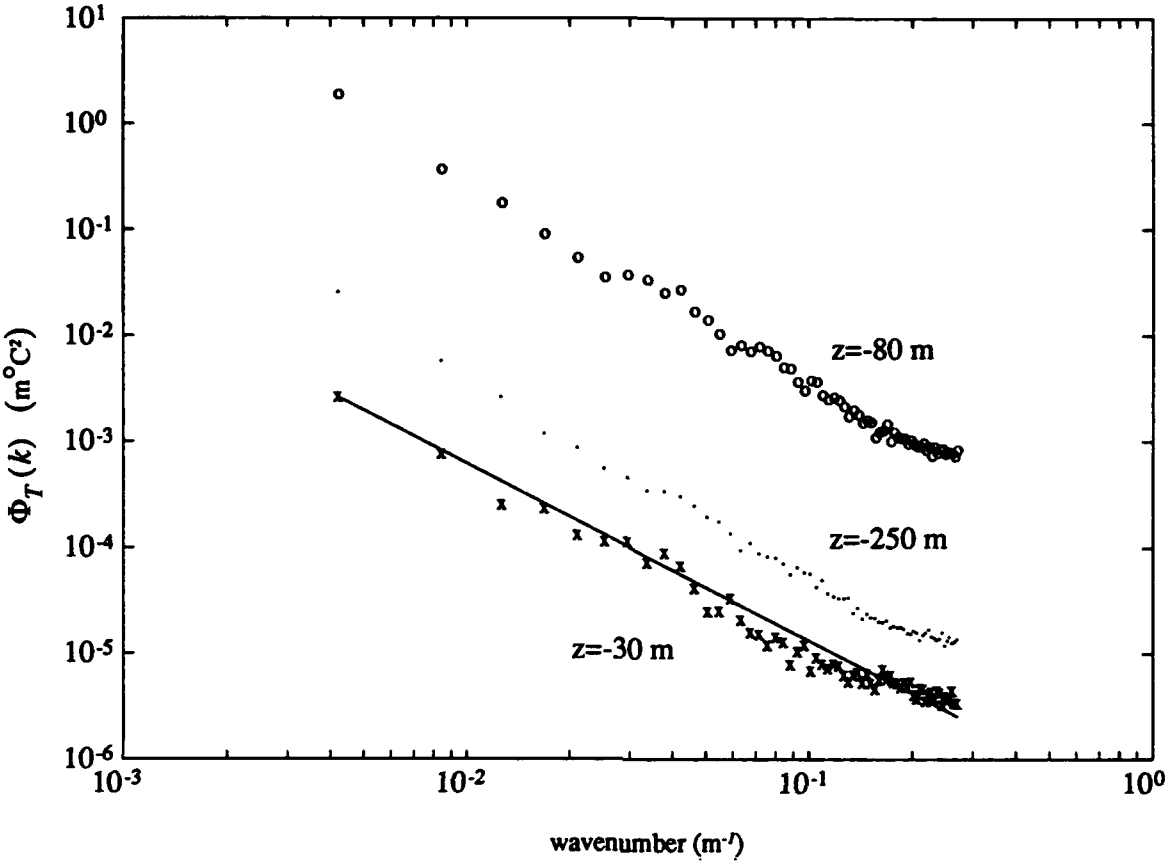

Fig 5. Temperature spectra within the OML (30 m), deep in the thermocline (250 m), and shallow in the thermocline (80 m). A solid line shows the theoretical -5/3 power law for turbulence spectra.

III. ACOUSTIC PROPAGATION IN INHOMOGENEOUS WATER

Acoustic intensity $|\overline{p^2}|$ decays in a surface duct by $1/r$ because of cylindrical spreading. The low frequency cutoff is approximated by $\lambda_{max}=4.7\times10^{-3}h^{3/2}$ where λ_{max} is the wavelength of the cutoff frequency in feet and h is the depth of the OML in feet (Urick, 1983, p. 151). For this duct λ_{max} is 5.0 m and the cutoff frequency is 295 Hz.

A. WAVE EQUATION IN INHOMOGENEOUS OCEAN

Before we can determine the effects of temperature perturbations, it is necessary to show the validity of the homogeneous wave equation in a temperature varying surface duct. First we compare the influence of pressure perturbations on sound speed with the influence of temperature perturbations on the speed of sound. Next comes a derivation of the wave equation in a temperature varying ocean. The governing wave equation in this situation is not homogeneous. The term that makes the wave equation nonhomogeneous is caused by density differences in the media. Then we show why the variance of the scattered pressure due to temperature change is of greater importance than neglect of the inhomogeneous term.

In the OML, the influence of pressure perturbations on the index of refraction is much smaller than the influence of temperature perturbations on the index of refraction. When ΔT = 0.1 °C, $\frac{1}{c_0}\frac{(\partial c)}{\partial T}(\Delta T) = 3.1\times10^{-4}$. The greatest influence on the refraction index is due to pressure perturbations through surface gravity waves. When the composite sea surface peak to trough Δz=3 m, $\frac{1}{c_0}\frac{(\partial c)}{\partial z}\Delta z$ is 3.3×10^{-5} . For this reason pressure perturbations are not considered, and pressure is assumed a function of depth only.

We assume density of the media to vary in space and to be frozen in time. This is called "quasi-static" because density variations induce motion, but at a slower time scale than the duration of acoustic transmissions. Using the method of small perturbations, we superimpose a sound field over the ambient density and pressure

$$\rho = \rho_0(x,y,z) + \rho_S(x,y,z)$$

$$p = p_0(z) + p_S(x,y,z)$$

We start with the equation of motion neglecting Coriolis and temporarily disregarding viscous effects

$$\rho d_t \hat{v} = -\nabla p - \rho g \hat{k} \tag{3.1}$$

which can be expanded as

$$(\rho_0 + \rho_S)\,[\partial_t \hat{v} + \hat{v} \bullet \nabla \hat{v}\,] = -\nabla p_0 - \nabla p_S - (\rho_0 + \rho_S)\, g \hat{k}$$

Since $\rho_S \ll \rho_0$, to the first order

$$\rho_0 \partial_t \hat{v} = -\partial_z (p_0) - \nabla p_S - \rho_0 g \hat{k}$$

Subtracting out the hydrostatic approximation leaves

$$\rho_0 \partial_t \hat{v} = -\nabla p_S \tag{3.2}$$

The continuity equation states that

$$\partial_t \rho + \nabla \bullet (\rho \hat{v}) = 0 \tag{3.3}$$

Expanding this in terms of ρ_0 and ρ_S and retaining only first order terms leaves

$$\partial_t \rho_S + \nabla \bullet (\rho_0 \hat{v}) = 0 \tag{3.4}$$

Differentiating and combining (3.2) and (3.4) yields

$$\partial_{tt} \rho_S = \nabla^2 p_S \tag{3.5}$$

In this case the speed of sound varies in space but not in time just as does density. Since pressure is related to density by

$$d_t p = c\,(x, y, z)^2 d_t \rho$$

which can be rewritten

$$\partial_t (p_0 + p_S) + \hat{v} \bullet \nabla (p_0 + p_S) = c^2 [\partial_t (\rho_0 + \rho_S) + \hat{v} \bullet \nabla (\rho_0 + \rho_S)\,]$$

Neglecting small terms leaves

$$\partial_t (p_s) = c^2 [\partial_t (\rho_S) + \hat{v} \bullet \nabla \rho_0]$$

Differentiating with respect to time and rearranging gives

$$\frac{1}{c^2} \partial_{tt} (p_S) = \partial_{tt} (\rho_S) + (\partial_t \hat{v}) \bullet (\nabla \rho_0) \tag{3.6}$$

Equations (3.5) and (3.6) are now combined to give

$$\frac{1}{c^2}\partial_{tt}(p_S) = \nabla^2 p_S + (\partial_t \vec{v}) \bullet (\nabla \rho_0)$$

Using the relationship in (3.2) enables this to be rewritten

$$\frac{1}{c^2}\partial_{tt}(p_S) = \nabla^2 p_S - \frac{\nabla \rho_0}{\rho_0} \bullet \nabla p_S$$

$$\frac{1}{c^2}\partial_{tt}(p_S) = \nabla^2 p_S - [\nabla ln(\rho_0)] \bullet \nabla p_S \qquad (3.7)$$

The first two terms are recognizable as the acoustic wave equation in the absence of temperature variability. The additional term results from the media density varying spatially. This equation is solved by acoustic pressure $p_s = p_0 + p_1$ where p_0 is a plane wave

$$p_0 = Ae^{i(\omega t - kx)}$$

and p_1 is the scattered wave. Chernov (1960) shows that the scattered wave is solved by

$$p_1 = -\frac{A}{4\pi}\int_V \left((2k^2 \frac{1}{c}(\frac{\partial c}{\partial T})_{p_0} \Delta T + \frac{ik}{\rho_0}(\frac{\partial \rho}{\partial T})_{p_0} \partial \frac{(\Delta T)}{\partial \xi} \right) \frac{1}{r} e^{ik(r+\xi)} dV$$

where

A is the amplitude of the incident wave

k is the wavenumber of the acoustic transmission

r is the distance from a scattering element to the receiver (x,y,z) coordinate

ξ is the distance from source to the scattering element, and

V is the scattering volume.

In this case V is the entire media between source and receiver. Acoustic fluctuations due to temperature perturbations are found from the variance of the scattered pressure $|\overline{p_1}|^2$. This is

$$|\overline{p_1}|^2 = V\left(\frac{A(\Delta T)k^2}{2\pi r}\right)^2 \left[\frac{1}{c_0}(\frac{\partial c}{\partial T})_{p_0} + \frac{1}{\rho_0}(\frac{\partial \rho}{\partial T})_{p_0} \sin^2\frac{\theta}{2}\right]^2 \int_V N(\vec{r}) e^{i(\vec{K}\cdot\vec{r})} dV \quad (3.8)$$

Here, $N(\vec{r})$ describes the correlation distance of inhomogeneities in the media. Both terms in brackets are caused by temperature variance. The first term in the brackets is due to sound velocity perturbations and the second term in the brackets is due to density perturbations. Relative size calculations for the 11 October data

show term 1 $\approx 3.1 \times 10^{-3}\ ^{\circ}C^{-1}$. If the scattering angle θ is less than 90 degrees, term 2 is less than $\approx 9.8 \times 10^{-8}\ ^{\circ}C^{-1}$ and can be disregarded. Neglect of the second term in the brackets of equation (3.8) is equivalent to neglect of $[\nabla ln(\rho_0)\ ] \bullet \nabla p_S$ in (3.7) (Ibid, p. 50). This reduces the wave equation in a quasi-static ocean with small temperature perturbations to the familiar homogeneous wave equation

$$\frac{1}{c^2}\partial_{tt}(p_S) = \nabla^2 p_S \tag{3.9}$$

B. PARABOLIC WAVE EQUATION

Separation of variables isolates the time dependence of equation (3.9). What is left is the Helmholtz equation. Dropping the subscript s, this is written

$$\nabla^2 p + k^2 p = 0$$

Expressed in cylindrical coordinates, the Helmholtz equation is

$$\partial_{rr}p + \frac{1}{r}\partial_r p + \partial_{zz}p + (k_0 n)^2 p = 0 \tag{3.10}$$

where $k_0 = (2\pi f)/c_0$ and $n(r, z) = c_0/(c(r, z))$ is the local index of refraction. This is an elliptic wave equation. Tappert (1974) introduced the parabolic equation approximation (PE) to underwater acoustics. Again, using separation of variables, let the sound pressure field have the form

$$p(r, z) = \frac{A(r, z)}{\sqrt{r}} V(r) \tag{3.11}$$

Here, $1/(\sqrt{r})$ contains the decay due to cylindrical spreading. $V(r)$ contains the rapidly varying component of the pressure field. It is solved by the Hankel function, which is approximated in the far field by

$$V = \sqrt{\frac{2}{\pi k_0}} e^{i(k_0 r - \frac{\pi}{4})}$$

$A(r, z)$ is the slowly varying component of the pressure field. It contains all of the depth dependence. $A(r, z)$ is the envelope of sound pressure that the IFD-PE model solves. Applying the solution for $p(r, z)$ to (3.11) and disregarding all terms that diminish more rapidly than $1/(\sqrt{r})$ gives

$$\frac{V}{\sqrt{r}}\left(-k_0^2 A + \partial_{rr}A + 2ik_0\partial_r A + \partial_{zz}A + (k_0 n)^2 A\right) = 0$$

dividing by $r^{-1/2}V$ yields

$$k_0^2(n^2-1)A + \partial_{rr}A + 2ik_0\partial_r A + \partial_{zz}A = 0$$

If it holds that $\partial_{rr}A \ll 2ik_0\partial_r A$ then

$$k_0^2(n^2-1)A + 2ik_0\partial_r A + \partial_{zz}A \approx 0 \qquad (3.12)$$

This is the most widely used parabolic wave equation in underwater acoustics. This approximation is valid when the backscattered field is negligible and ray bundle travel is predominantly horizontal. This condition is easily met in the OML. The PE accurately governs acoustic propagation in a surface duct.

IV. ACOUSTIC SIMULATION

The acoustic propagation model developed by Lee and McDaniel (1987) applies a finite difference numerical scheme to the PE of Tappert. Finite differencing enables the governing equation to be converted from a boundary value problem to an initial value problem in which the solution marches horizontally. This means that the pressure field at range $r + \Delta r$ is determined entirely by the pressure field at range r. Because the model solution marches, it is feasible to modify the sound velocity profile at the very short ranges of the thermistor data collection. Lee and McDaniel apply an "implicit" finite difference algorithm. Implicit finite difference schemes have the advantage of unconditional stability. The model is referred to in this paper as the IFD-PE.

The IFD-PE acoustic transmission model was run at several frequencies between 500 Hz and 10 kHz in both a horizontally temperature varying and temperature invariant ocean medium. Since the IFD-PE model algorithm marches horizontally it is especially well suited to accepting horizontal changes in sound speed. The accuracy of finite difference techniques is tied to range step size. Lee and McDaniel (1987, pp. 341-349) devote an entire chapter to range step size analysis. They show an optimum choice for range step in the IFD-PE is 1/2 of the wavelength of the acoustic frequency. This is the range step used for all simulations of acoustic propagation in this thesis. For 500 Hz it is 1.48 m and for 10 kHz it is 7 cm. The range step is modified every 1.852 m to make the marched acoustic pressure field coincident with the input of each SVP. An example of range stepping for a 500 Hz source is sketched below.

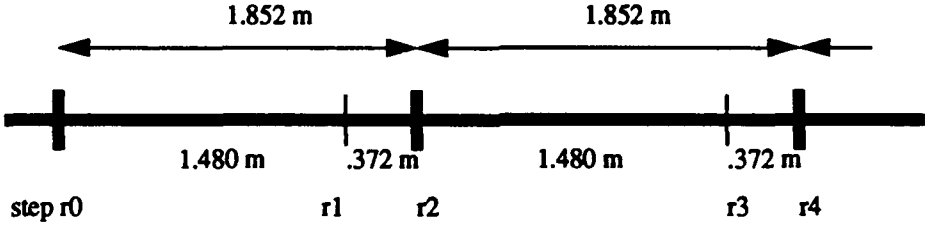

Fig 6. Step size of the IFD-PE model for a 500 Hz sound source.

The same range step size is used for both the varying and non varying cases so that the only difference in the sound field is due entirely to perturbations in sound speed caused by temperature variations.

A. ASSUMPTIONS IN THE COMPUTER SIMULATION

1. Temporally Frozen

There are two separate assumptions about the time variance of this simulation. The first is in the thermistor chain data collection. An actual two dimensional temperature field must be measured at all grid points simultaneously. This data set is assumed to represent a typical instantaneous snapshot of an OML with 45 km in length. The precise deterministic paths of ray bundles are different, but the statistics of acoustic propagation are as if all temperature readings had been taken simultaneously.

A separate assumption is that the water is static for the duration of the sound propagation event. To understand this assumption it is useful to separate water motions into two categories. Large scale motions like currents and tides advect the entire transmission path and therefore do not affect acoustic propagation. Small scale motions have a couple of effects. They advect patches of water of varying temperature, thus continuously modifying the sound speed at each location. They also impart relative speed to acoustic transmissions. The sound speed in the ocean is about 1500 m/s and the speed of small scale motions is typically less than 10 cm/s. Although they are five orders of magnitude smaller than the speed of sound, they impart enough velocity to the acoustic energy to create a doppler shift. Material velocity variations usually have a smaller effect on acoustic transmission than do temperature variations, but they are not altogether negligible (Neubert, 1970; Flatté, 1979, p. 86). The assumption of static water motion is called "Taylor's hypothesis" (Flatté, 1979, p. 101). It is consistent with work done by Chernov (1960, p. 36) among others.

2. Artificial Absorbing Bottom

In ocean acoustics there are several deterministic paths ray bundles may follow between source and receiver. In a typical ocean environment sound energy that refracts out of the surface duct at sufficiently small angles relative to the horizontal plane is refracted downward by the underlying thermocline. Below the thermocline the vertical temperature gradient becomes small. Furthermore, the sound speed increases with pressure, and therefore, the sound speed increases with depth. The combination of deep near-isothermal water and increasing pressure refracts rays toward the horizontal. If there is sufficient depth, sound energy is refracted past horizontal and continues up to the surface. This mode of propagation is called convergence zone (CZ). Sound energy that leaves the surface duct at steeper grazing angles interact with the bottom. There they are partially reflected, partially absorbed, and partially refracted through the ocean floor. Energy reflected from and refracted through the ocean bottom returns to the surface. This is called the bottom bounce (BB) mode of propagation. Both BB and CZ energy exit and then reenter the surface duct. The remaining

propagation paths are surface reflected at shallow angles and direct path (DP). These modes remain continuously in the surface duct.

CZ and BB propagation is excluded from the solution by introducing an artificial absorbing bottom. This is accomplished in the IFD-PE model with an algorithm that extends the bottom by 4/3 of the depth of the sound field with a large attenuation coefficient. Acoustic energy refracted or diffracted from the surface duct continues downward because of the thermocline. It interacts with and is attenuated by this bottom. This algorithm eliminates all but surface duct propagation from the solution.

Introduction of an artificially absorbing bottom has one drawback and three overriding positive aspects. The drawback is the artificiality introduced. This is only a minor difficulty. Surface duct propagation is easily resolvable from BB/CZ in the real world. The primary advantage is that BB and CZ propagation do not clutter the results. Since they contribute to the ensonification of the surface duct at intermittent intervals, they would be a source of noise for this simulation. Another advantage is the reduction in computer time attained by modeling only the upper 250 m. A 16 fold increase in depth would result in a 16 fold increase in computer time. The other advantage to a completely absorbing bottom is the difficulty it eliminates by determining how to most realistically model the bottom. The coefficient of reflection is highly dependent on bottom type and density.

3. Gaussian Starting Field

The PE model is valid only in the far field $(r \gg \frac{\lambda}{2\pi})$. It needs a starting field well removed from the source. A starting field can be generated by a ray tracing model or a normal mode solution to the nonhomogeneous wave equation. A much simpler initial field suitable for our purposes, however, is derived by Tappert (1977). The starting field consists of a Gaussian distribution of pressure in the vertical. The Gaussian distribution is constrained by an asymptotic approximation to the solution of the nonhomogeneous wave equation for a point source. The error induced by this approximation to a point source is negligible at distances far from the source.

4. Isohaline

As previously stated the speed of sound in water is controlled by temperature, salinity, and pressure. Thermistor chain data provides the temperature field. Chernov (1960) shows that the effect of

salinity perturbations on sound speed is typically one order of magnitude less than that of temperature perturbations. Therefore we neglect the influence of the salinity field.

5. Other Scatterers

There are several other scatterers of acoustic energy within the OML not addressed in this simulation. Surface gravity waves and chop reflect sound energy out of the OML and smear the frequency transmitted. Bubbles attenuate sound and modify the local speed of sound. Material movement of the medium creates a doppler shift that also blurs the frequency. Even biologics scatter sound. These scatterers probably have a greater influence on sound speed fluctuations than do temperature perturbations for medium frequencies. Medwin (1973) found that the predominant cause of acoustic phase fluctuations at 24.4 kHz and 95.6 kHz is bubble activity rather than temperature perturbations. In measurements at sea, Nichols and Young (1968) found that at 270 Hz there were peak fluctuations at the short range (2 nm) and the long range (700 nm) probably corresponding to surface waves. They also found that for long range only there were peak fluctuations of 0.1 hr^{-1} to 0.01 hr^{-1} probably corresponding to internal waves. Urick and Tulko (1969) transmitted frequencies between 750 Hz and 1500 Hz over 24 nm in the deep sea to determine the spatial correlation for bottom mounted receiver separations up to 300 ft, and they found that the correlation was unaffected by wind speed and sea roughness, even though the transmission path was surface reflected. Urick (1973) concluded that the major factors causing decorrelation of vertical coherence from a near surface source are i) interference of the direct path with the reflected path, ii) temperature and salinity perturbations, and iii) the effect of multiple surface and bottom reflections.

B. STATISTICS OF ACOUSTIC PROPAGATION THROUGH OML

There are many different ways to characterize the sound field. Units of decibels (db), acoustic intensity, or absolute acoustic pressure are all equivalent. Because transmission loss generally vacillates several orders of magnitude, acousticians often translate absolute acoustic pressure P_a to a logarithmic scale and use db. The transmission loss in db experienced at any (range, depth) coordinate is thereby computed as $TL=20\log(P_a)$. In this discussion acoustic energy is everywhere referenced to a source of 1 sound pressure unit. Absolute acoustic pressure, therefore, is dimensionless.Transmission loss curves are generally plotted at a single receiver depth as a function of range. They display the slowly varying component of the solution to the wave equation. The rapidly varying component $e^{i(kr-\omega t)}$ is separated from the transmission loss curve. Figure

7 is a curve of this type. It shows the decay of sound energy due to cylindrical spreading in the surface duct. The sound pressure fluctuates about a mean value that is a function of range. In this case the source and receiver depths are both 35 m. The curve has limited value because it fails to describe what the acoustic pressure is at any other receiver depth. Also, it describes acoustic fluctuations inadequately.

A more elaborate representation of the acoustic pressure field is given by statistical analysis. We need both average acoustic pressure and the spatial variation of acoustic pressure. Acoustic pressure was recorded at each 2 m by 2 m gridpoint for 400 m at each sample range (20 km, 40 km, 60 km, 80 km, and 100 km). Acoustic pressure samples are only taken at isolated ranges rather than averaged together over the whole range of the transmission because acoustic pressure depends on range. That is, acoustic propagation is not a

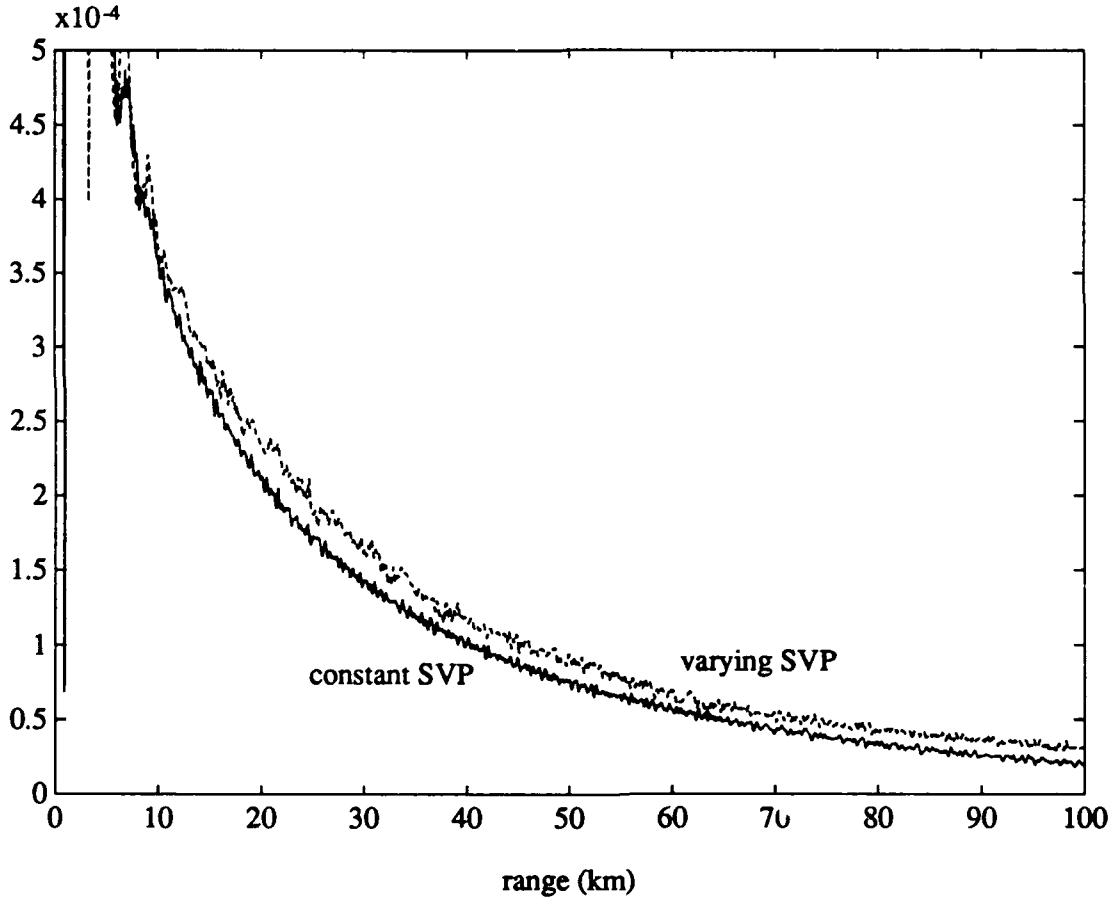

Fig 7. Normalized sound pressure as a function of range for a 500 Hz source. In both cases the acoustic pressure is determined for a 35 m source and receivers at 35 m. The first order decay of acoustic intensity with range is due to cylindrical spreading.

stationary process. For purposes of comparison, however, it is assumed to be stationary for a 400 m stretch of ocean.

The horizontally averaged acoustic pressure as a function of depth is shown in Fig 8 through Fig 13. Each figure corresponds to a monofrequency source from 500 Hz to 10 kHz. The source was located at 35 m depth. The plots display average absolute acoustic pressure at range 20 km and 100 km. Average acoustic pressure in the idealized surface duct is shown with a solid line, and in the temperature varying surface duct is shown as a dashed line. The figures show the strong depth dependence of acoustic pressure. The maxima and minima demonstrate the depth dependent normal modes. Higher frequencies have more modes. At some frequency-depth-range combinations, sound pressure is higher in a temperature invariant OML. At other frequency-depth-range combinations, the situation is reversed.

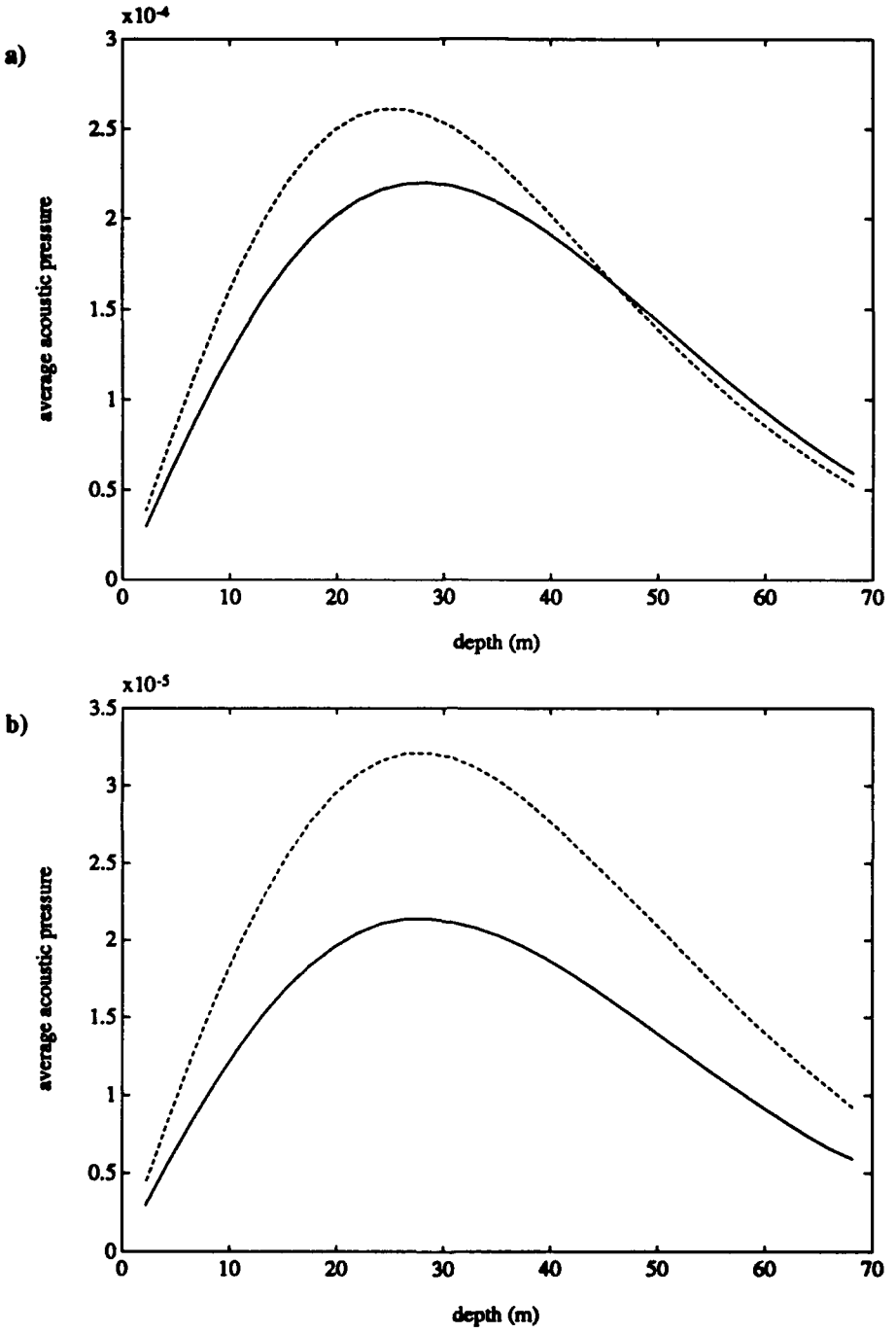

Fig 8. Depth dependence of average acoustic pressure for a 500 Hz source at range a) 20 km and b) 100 km. The source is at 35 m depth in the surface duct. Solid lines show average acoustic pressure in a temperature invariant OML. Dashed lines show average acoustic pressure in a temperature varying OML.

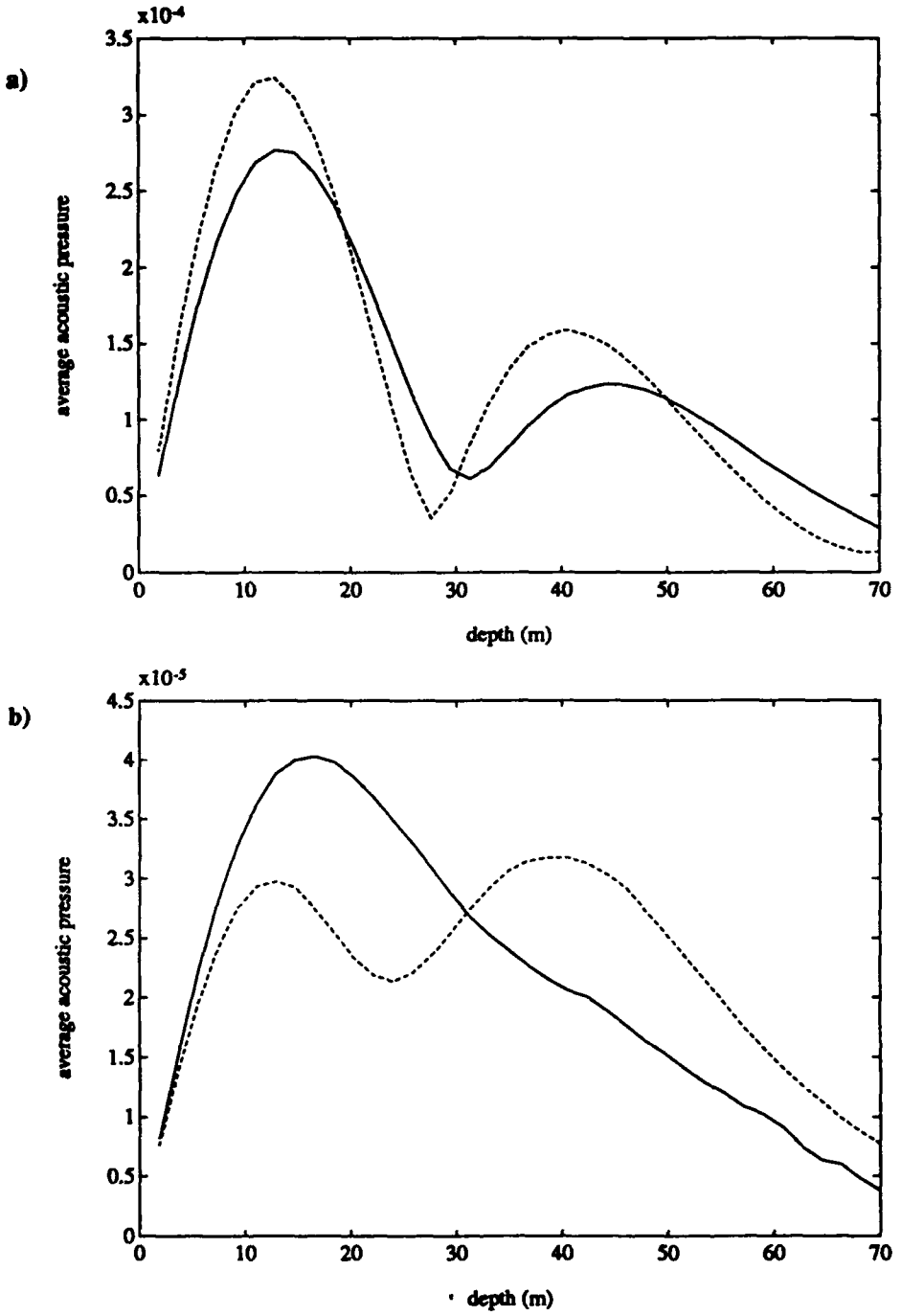

Fig 9. Depth dependence of average acoustic pressure for a 1 kHz source at range a) 20 km and b) 100 km. The source is at 35 m depth in the surface duct. Solid lines show average acoustic pressure in a temperature invariant OML. Dashed lines show average acoustic pressure in a temperature varying OML.

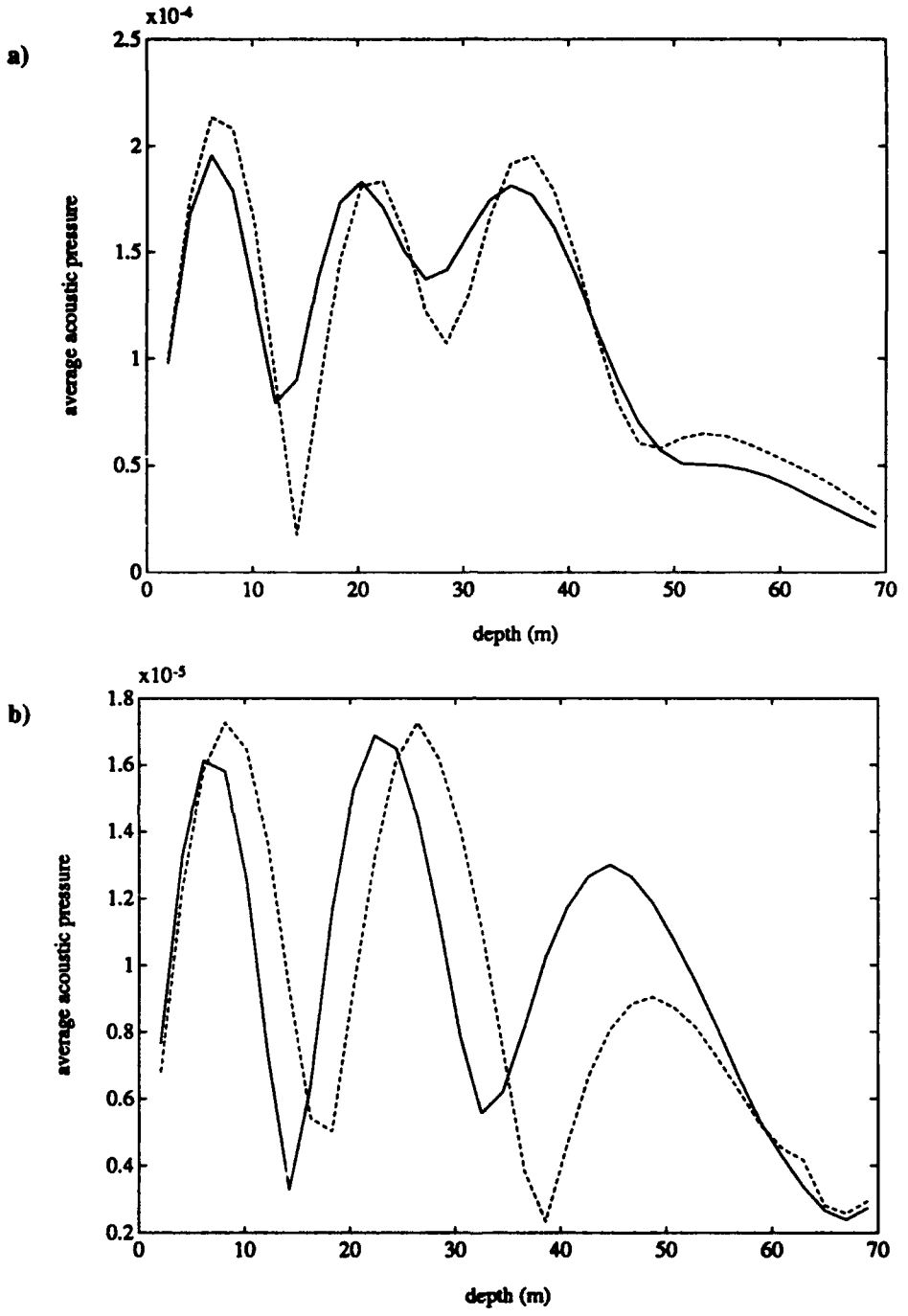

Fig 10. Depth dependence of average acoustic pressure for a 2 kHz source at range a) 20 km and b) 100 km. The source is at 35 m depth in the surface duct. Solid lines show average acoustic pressure in a temperature invariant OML. Dashed lines show average acoustic pressure in a temperature varying OML.

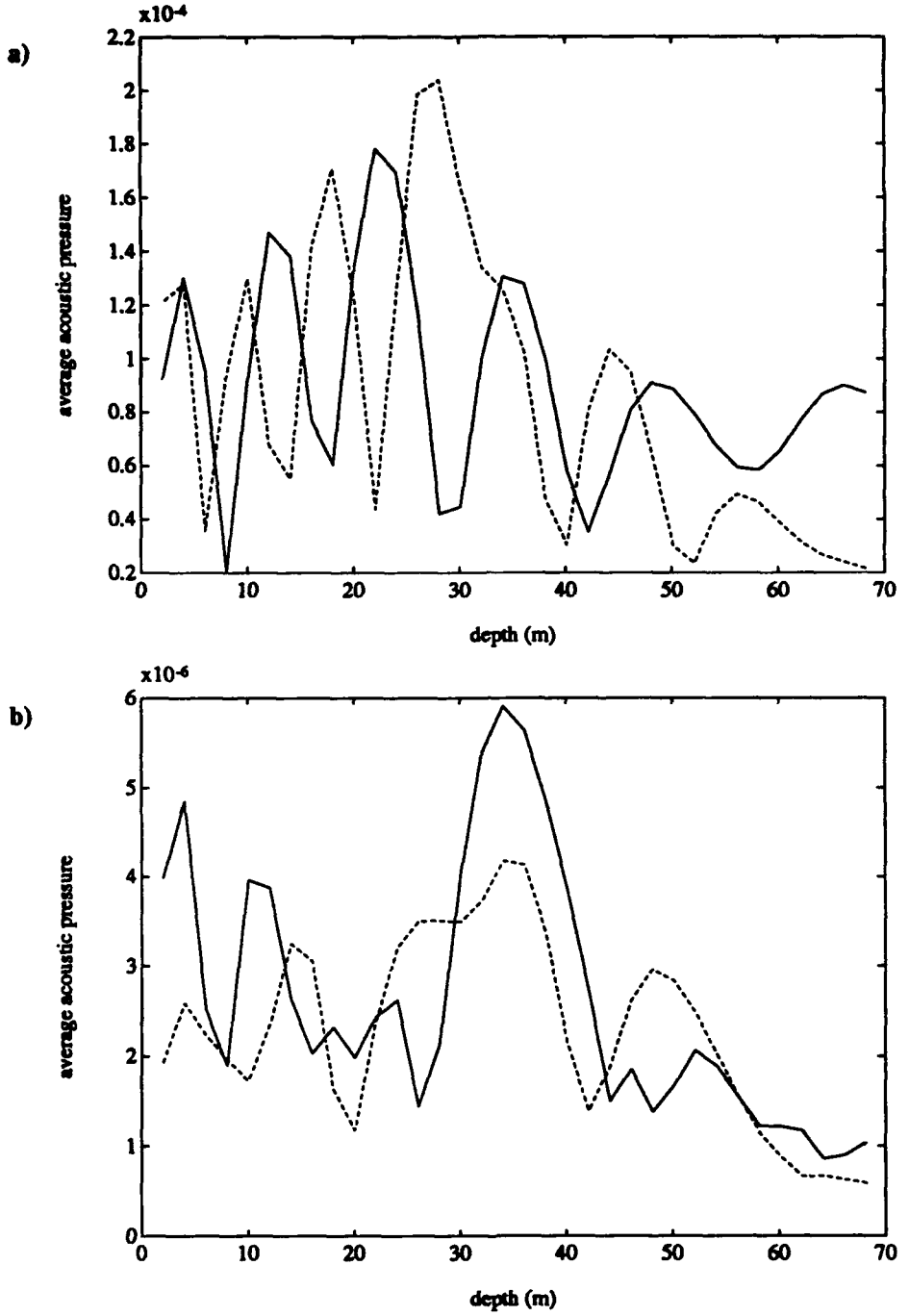

Fig 11. Depth dependence of average acoustic pressure for a 3.5 kHz source at range a) 20 km and b) 100 km. The source is at 35 m depth in the surface duct. Solid lines show average acoustic pressure in a temperature invariant OML. Dashed lines show average acoustic pressure in a temperature varying OML.

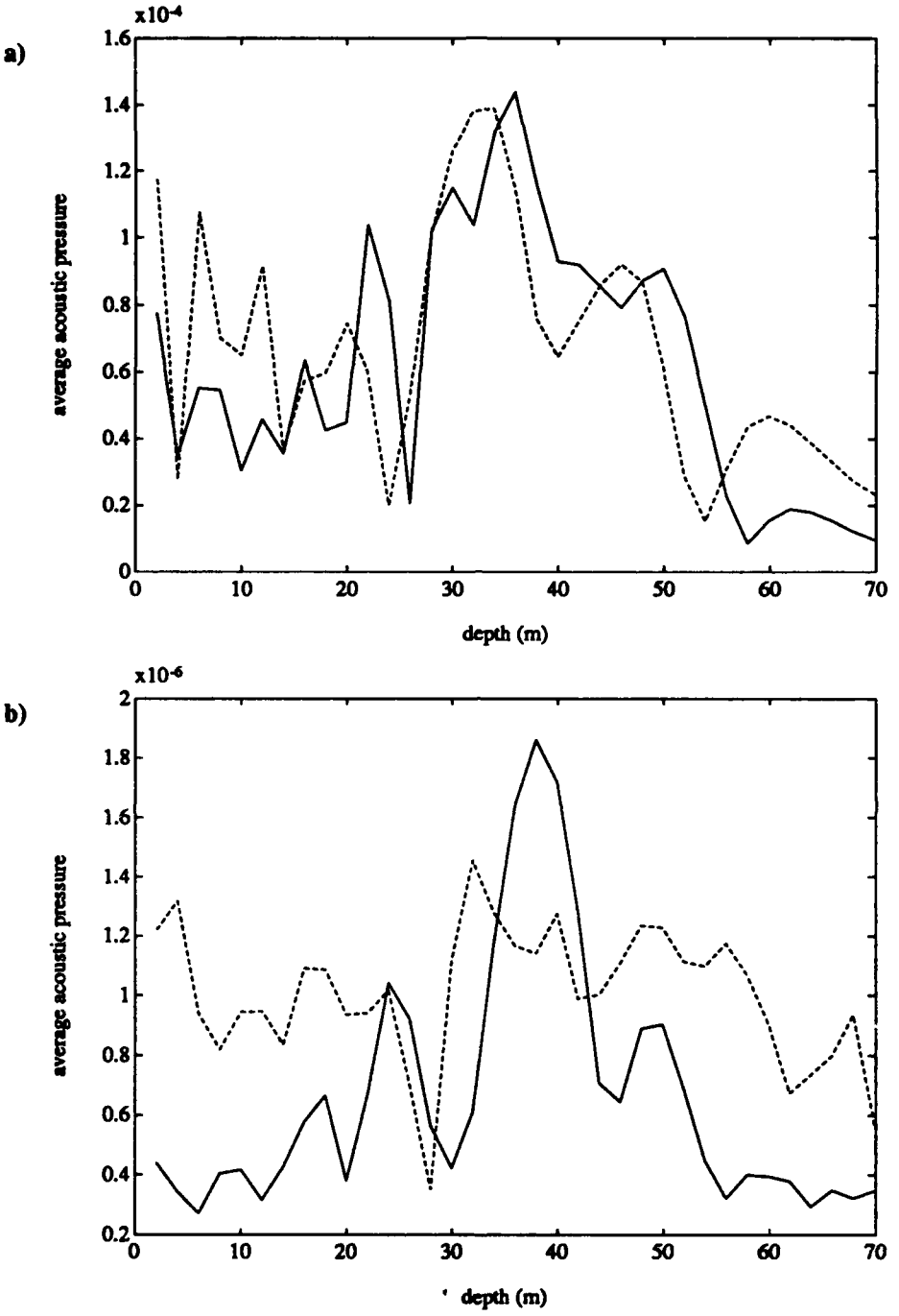

Fig 12. Depth dependence of average acoustic pressure for a 5 kHz source at range a) 20 km and b) 100 km. The source is at 35 m depth in the surface duct. Solid lines show average acoustic pressure in a temperature invariant OML. Dashed lines show average acoustic pressure in a temperature varying OML.

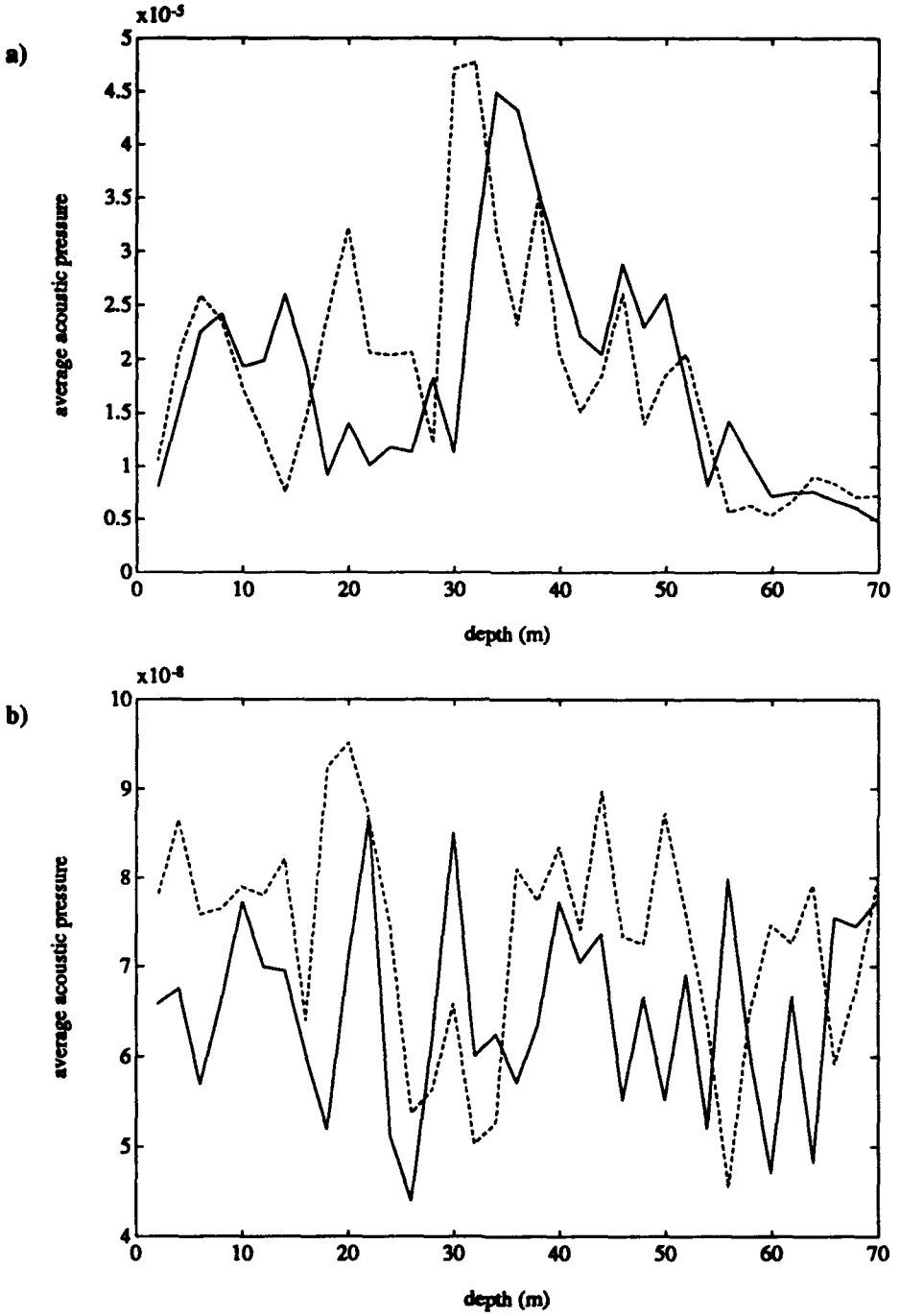

Fig 13. Depth dependence of average acoustic pressure for a 10 kHz source at range a) 20 km and b) 100 km. The source is at 35 m depth in the surface duct. Solid lines show average acoustic pressure in a temperature invariant OML. Dashed lines show average acoustic pressure in a temperature varying OML.

The average acoustic pressure characterizes the sound field incompletely. The spatial deviation of acoustic pressure is also of interest. Figure 7 is an example of how the slowly varying component of the solution to the wave equation does not vary very slowly. It is therefore necessary to perform a fast fourier transform on the acoustic pressure at each sample depth (2m to 70m). As seen from Fig 8 through Fig 13, acoustic propagation is modified by depth as well as range. However, for purposes of comparison, the spectra of acoustic fluctuations is assumed to be stationary in depth throughout the OML at each range. Averaging the spectra over depth increases the statistical reliability of the resultant acoustic fluctuation density curves. Any error induced by vertically averaging acoustic fluctuation spectra is the same for each case. An assumption of ergodicity at isolated ranges and through the depth of the OML enables comparison of sound fluctuations in an OML as a function of range, frequency, and temperature variance. They can be compared with a single parameter--the acoustic fluctuation density.

Figure 14 through Fig 19 show the acoustic fluctuation density for the six acoustic frequencies of this simulation. Spectra of acoustic fluctuations are displayed at ranges of 20 km and 100 km. Again, solid lines show computed results through an idealized OML, and dashed lines show computed results through a realistic OML. The spectra describe how, for a fixed instant, the slowly varying component of an acoustic transmission varies horizontally.

Comparison of the acoustic fluctuation density shows how acoustic propagation is impacted by horizontal temperature variation. At frequencies below 2 kHz, spectra of acoustic fluctuations in a temperature varying OML approximate the spectra of acoustic fluctuations in a temperature invariant OML. At frequencies above 2 kHz, the same peaks are apparent in the spectra, but with much different amplitudes.

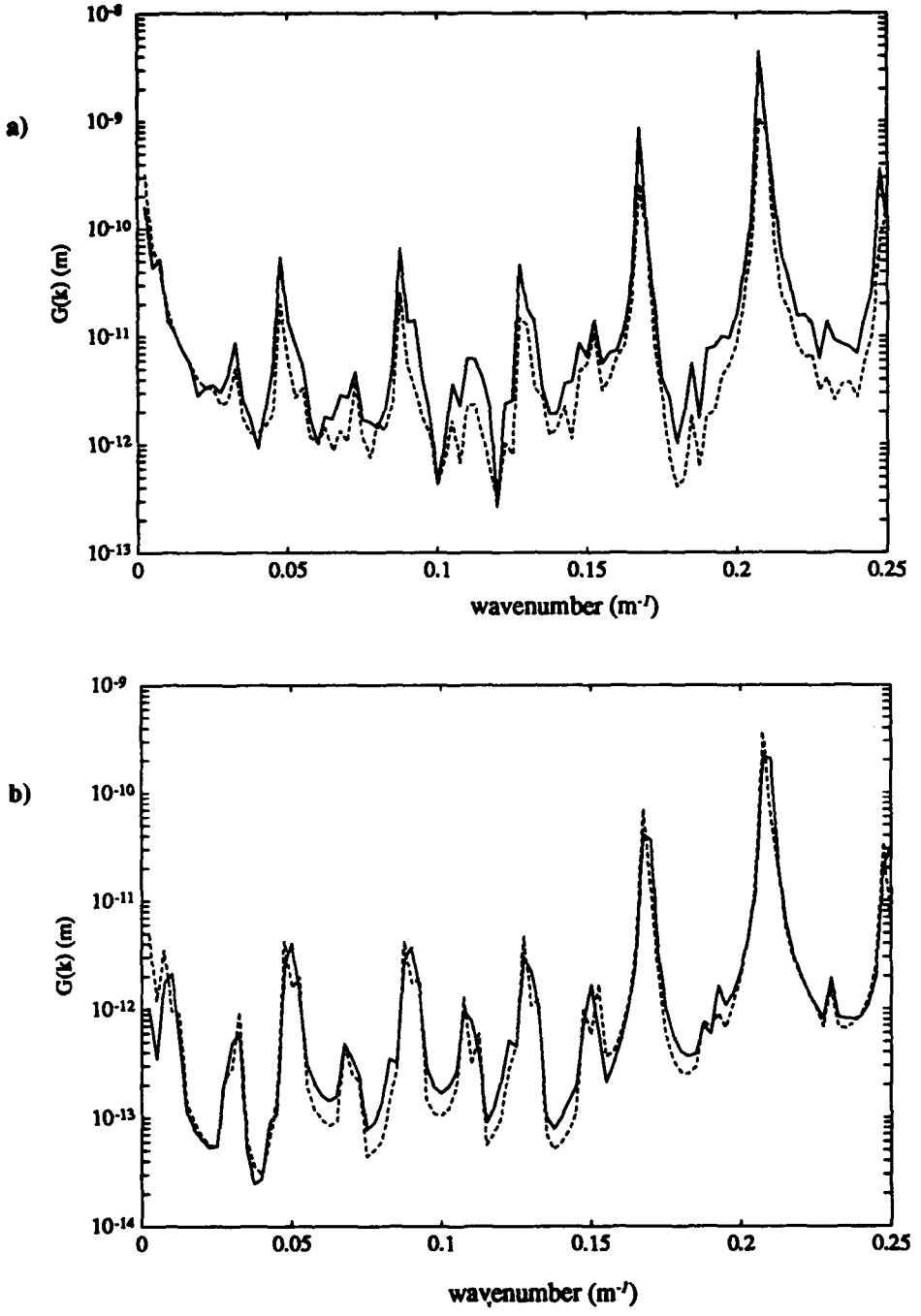

Fig 14. Energy density spectra of acoustic fluctuations due to 500 Hz source at range a) 20 km, b) 100 km.

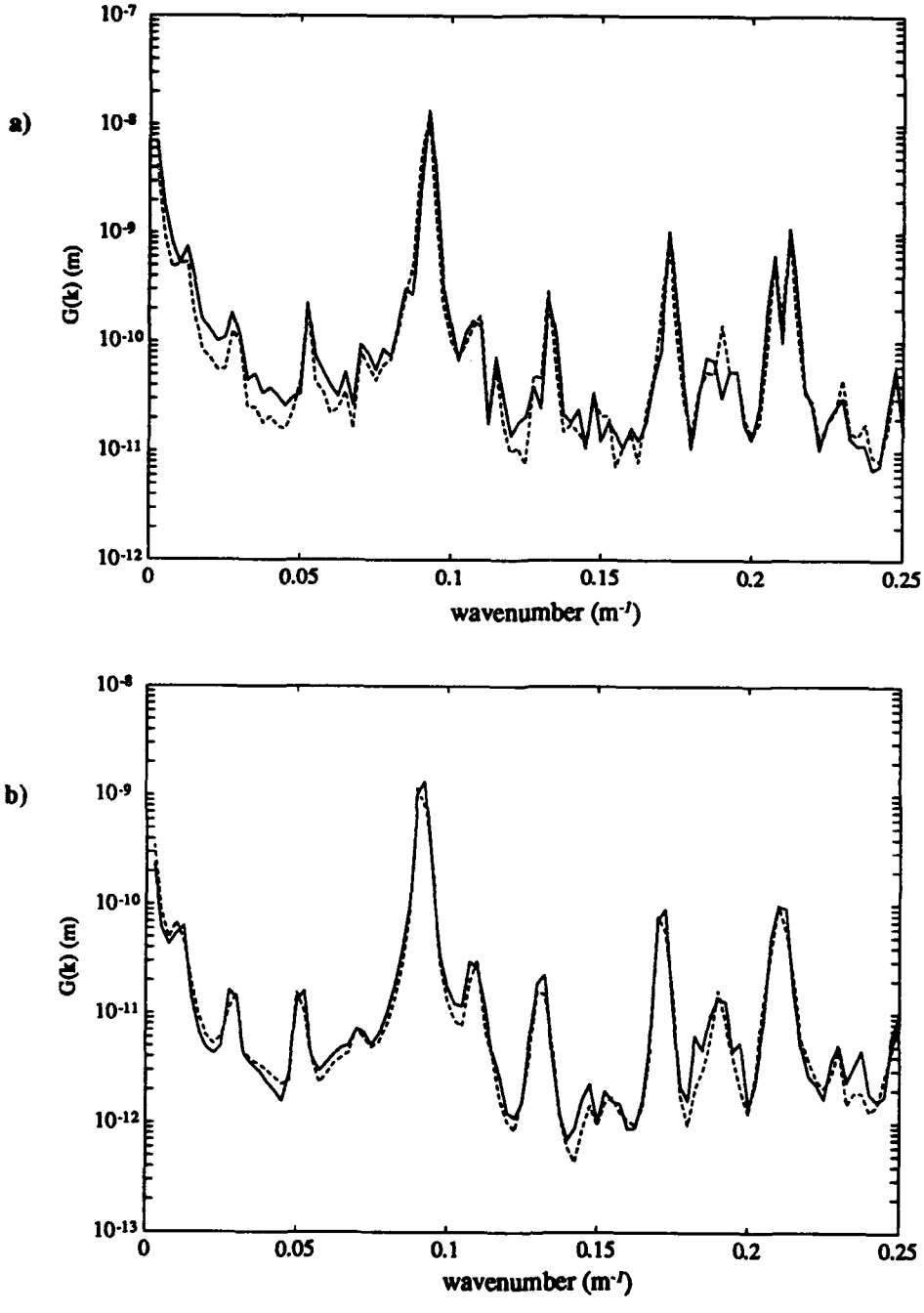

Fig 15. Energy density spectra of acoustic fluctuations due to 1 kHz source at range a) 20 km, b) 100 km.

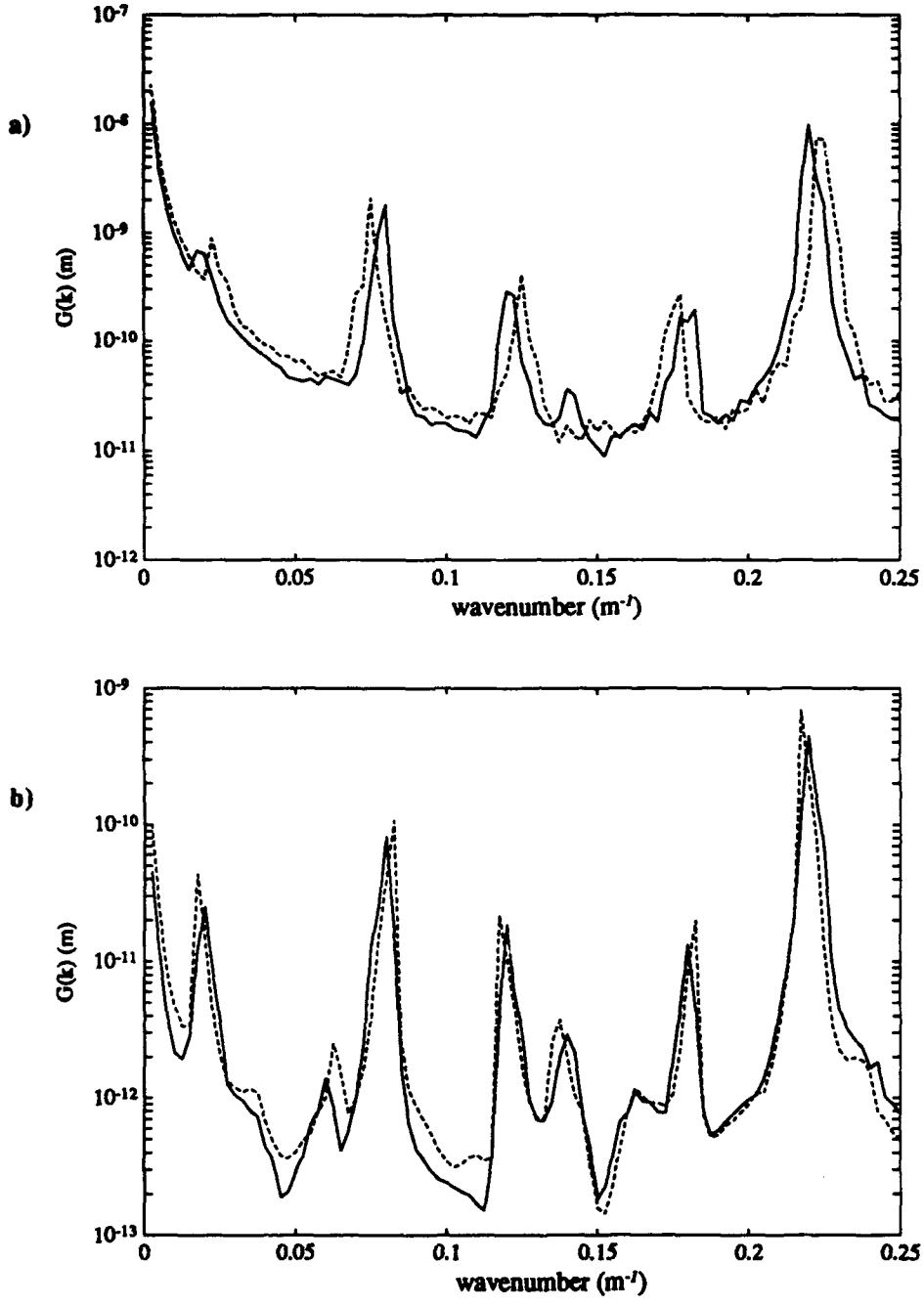

Fig 16. Energy density spectra of acoustic fluctuations due to 2 kHz source at range a) 20 km, b) 100 km.

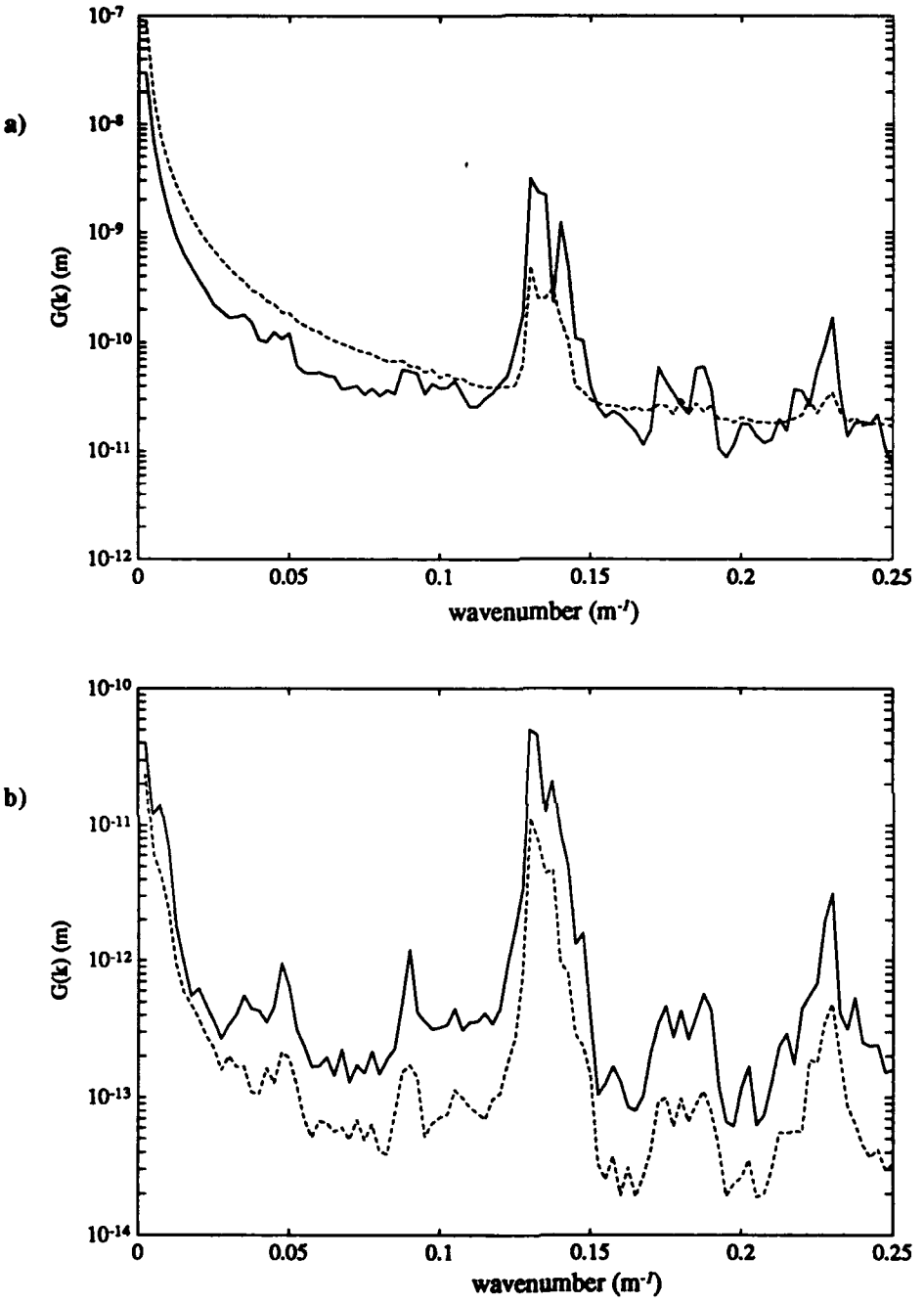

Fig 17. Energy density spectra of acoustic fluctuations due to 3.5 kHz source at range a) 20 km, b)100 km.

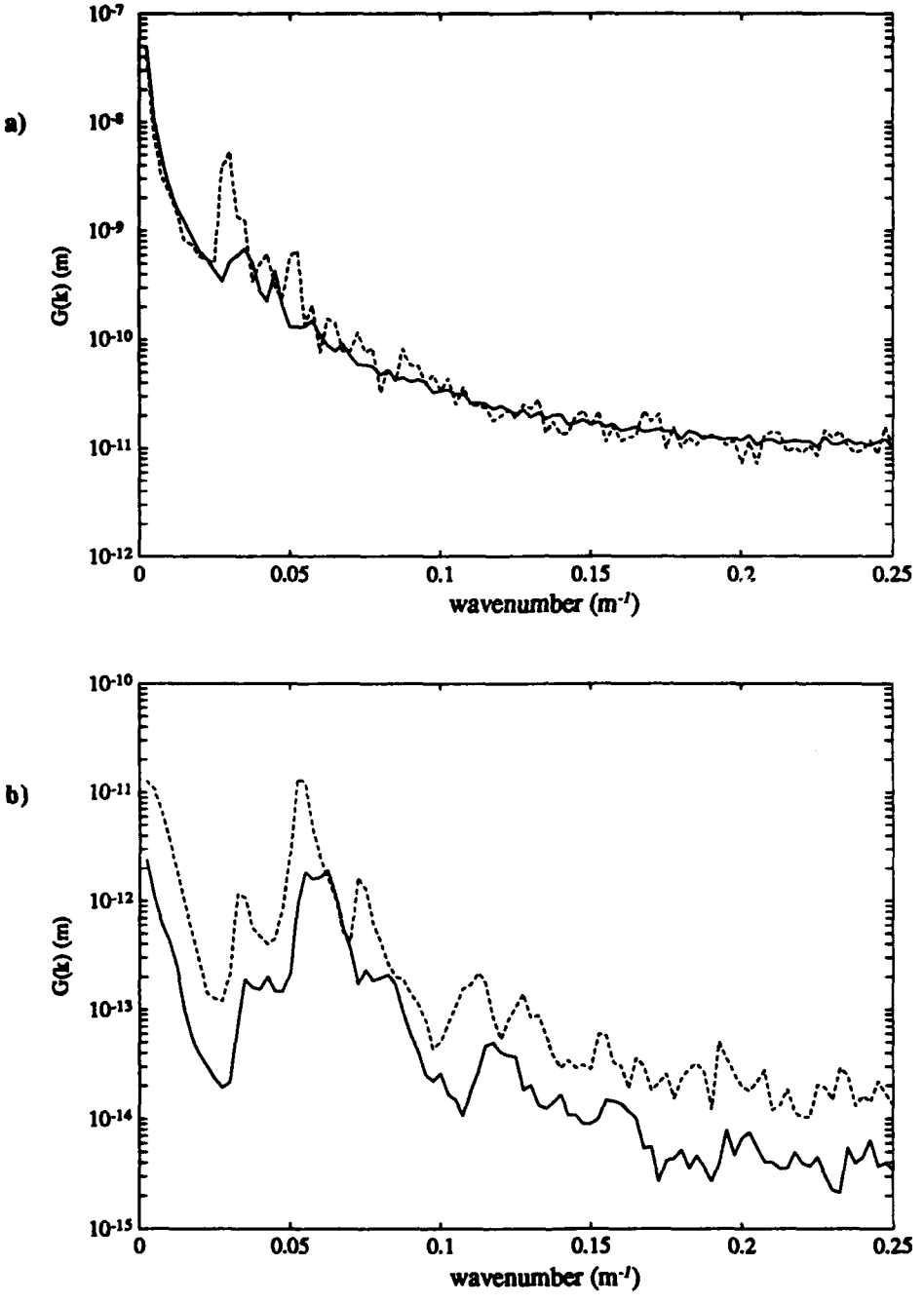

Fig 18. Energy density spectra of acoustic fluctuations due to 5 kHz source at range a) 20 km, b) 100 km.

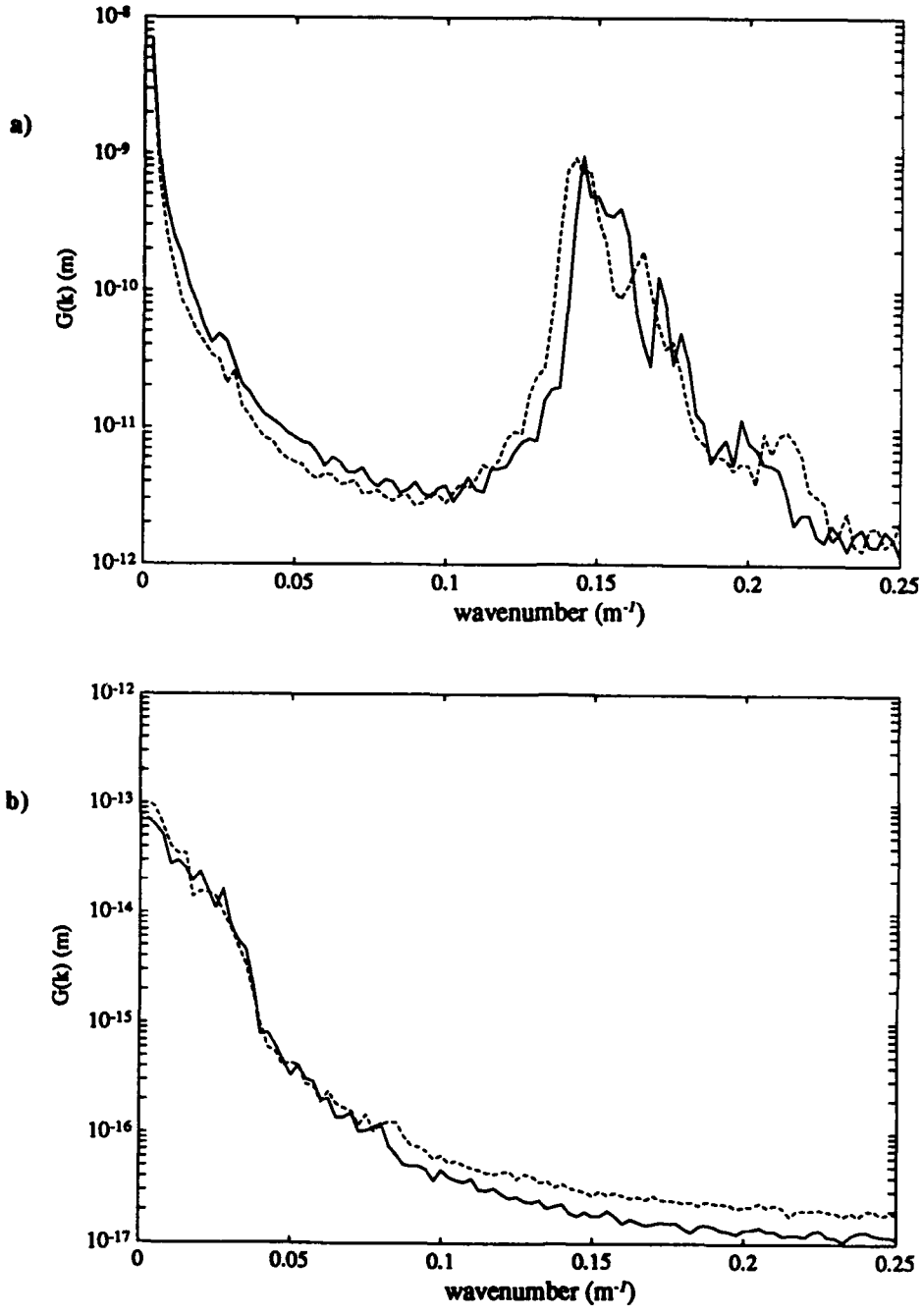

Fig 19. Energy density spectra of acoustic fluctuations due to 10 kHz source at range a) 20 km, b) 100 km.

V. DISCUSSION OF RESULTS

The sound field in this computer simulation is a function of several parameters. It depends on acoustic frequency, range, and finescale structure, and source depth. To compare the relative importance of each parameter, it is necessary to compute the overall average acoustic pressure and variance of acoustic pressure at each frequency and range. The average sound pressure is simply the mean of the depth dependent average acoustic pressure. The variance of acoustic fluctuations is found by integrating the spectra of acoustic fluctuations over all wavenumbers. This is analogous to integrating the transform of a time series to obtain a total variance. The variance of acoustic fluctuations is therefore depth averaged and wavenumber integrated. It represents a total spatial deviation from the mean acoustic transmission loss through the OML.

A. Range Dependence of Acoustic Propagation in a Surface Duct

Range dependence and frequency dependence of acoustic propagation through a surface duct are well understood. To a first approximation, acoustic transmissions decay with range due to cylindrical spreading in a surface duct by $1/(\sqrt{r})$ where r is the range. The average acoustic pressure at 5 ranges are plotted in Fig 20. They are compared with a solid line showing decay with range of $1/(\sqrt{r})$. More rapid decay is due to attenuation, scattering, and leakage out of the surface duct.

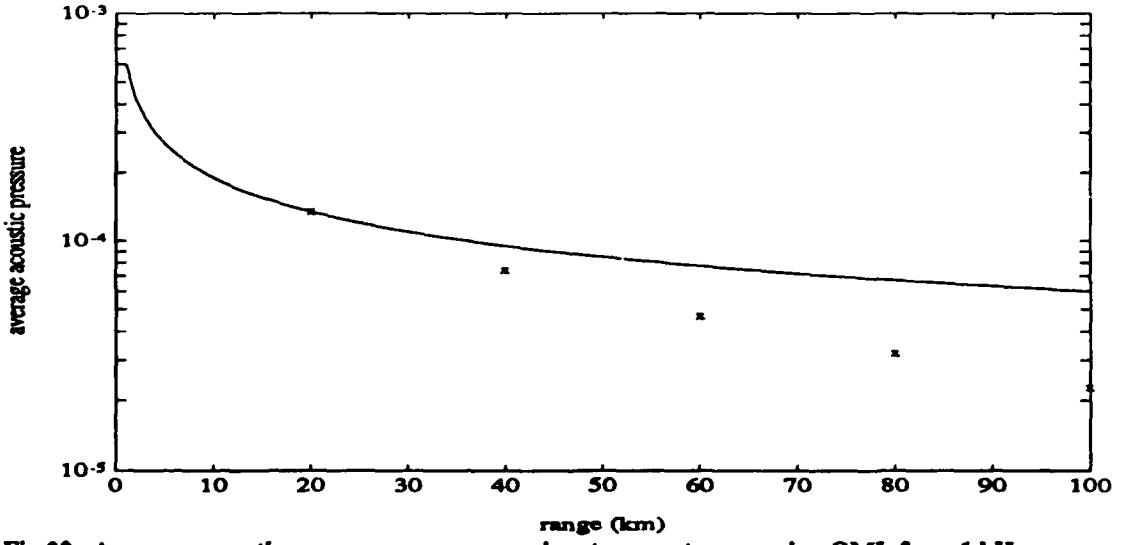

Fig 20. Average acoustic pressure versus range in a temperature varying OML for a 1 kHz source at 35 m depth. 'x' data points show computed average acoustic pressure. The solid line shows the theoretical rate of decay of acoustic energy with range due to cylindrical spreading in a surface duct.

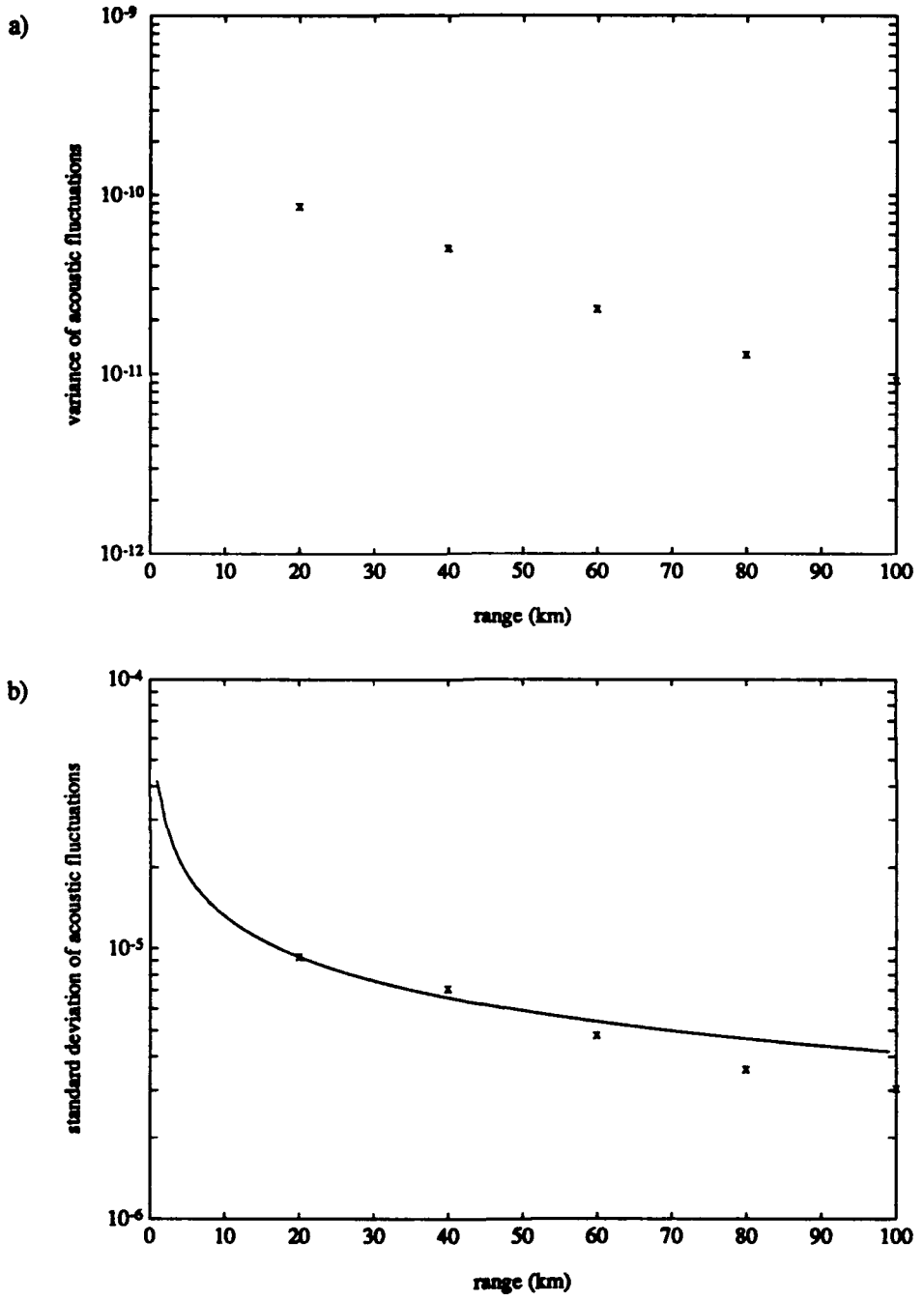

Fig 21. a) Variance of acoustic fluctuations with range for a 1 kHz source in a temperature varying OML at 35 m depth. In b) the standard deviation of acoustic fluctuations is compared to a solid line showing the rate of decay of average acoustic energy due to geometrical spreading in a surface duct.

Acoustic fluctuations appear to decay with range similar to the cylindrical spreading of average transmission loss. Figure 21a) has the acoustic fluctuation variance plotted for a 1 kHz source at 35 m depth in a temperature varying OML. Variance is computed every 20 km from 20 km to 100 km. Because it has the same units, a better parameter to compare with average transmission loss is the standard deviation of acoustic fluctuations. Figure 21b) shows the standard deviation of acoustic fluctuations. It is compared to a solid line showing decay of $1/(\sqrt{r})$. The solid line passes through the first value of standard deviation at 20 km. This figure demonstrates that acoustic fluctuations diminish less with range than average transmission loss does. Similar comparisons show that the ratio of standard deviation of sound pressure to average sound pressure increases with range at all frequencies.

B. Frequency Dependence of Acoustic Propagation through a Surface Duct.

Variance of acoustic fluctuations in this surface duct shows a predictable dependence on frequency. It has a maximum value that is a function of range as well as frequency. Figure 22 shows frequency dependence at 20 km and at 100 km. The source is at 35 m depth and sound propagates through a temperature varying OML. At 20 km, variance of acoustic fluctuations is the highest at 3.5 kHz. It is less at frequencies both higher and lower. The greatest variance at 100 km is at 1 kHz. This trend is predictable because it is very similar to the dependence of average transmission loss on frequency in a surface duct. Acoustic energy is leaked out of the duct at relatively low frequencies near the duct cutoff frequency. Acoustic energy at higher frequencies is lost by attenuation. Since acoustic fluctuations are driven by average acoustic energy, it is anticipated that variance of sound transmission adhere to similar frequency dependence.

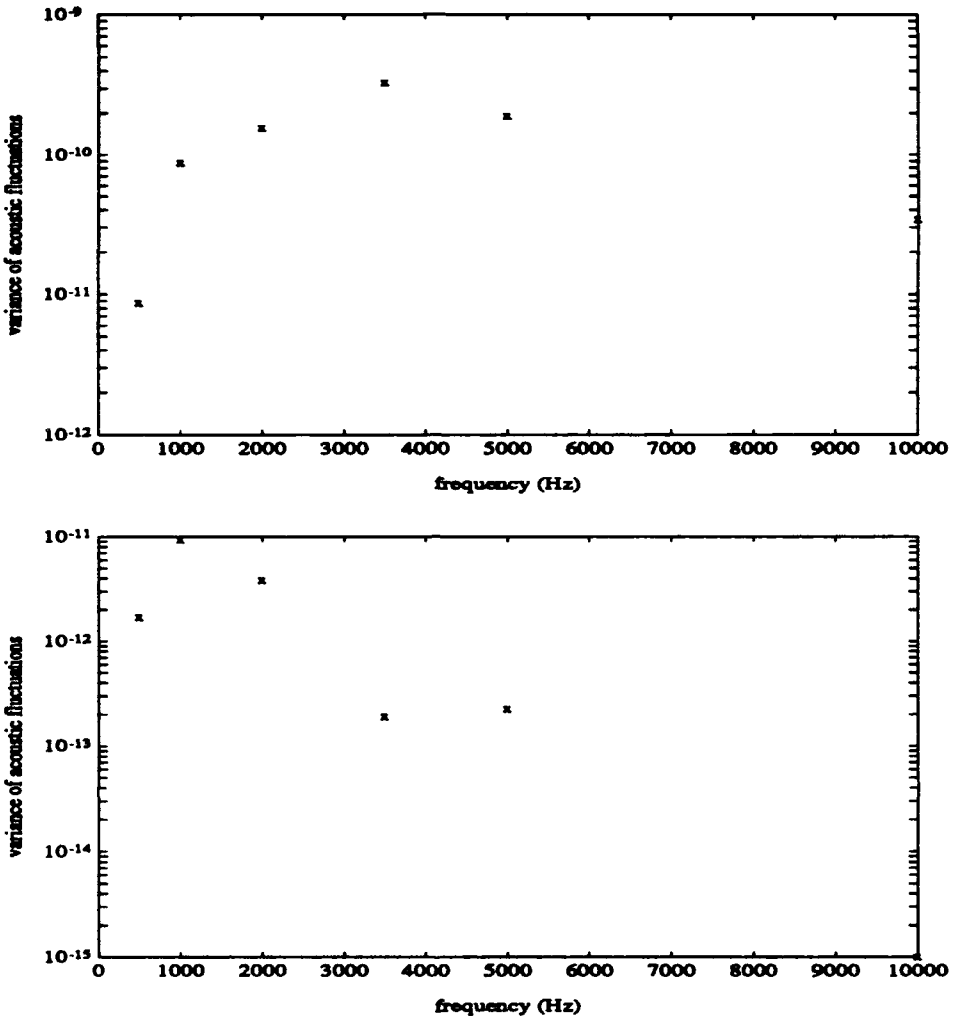

Fig 22. Variance of acoustic fluctuations versus frequency at range a) 20 km and b) 100 km. The sound source is at 35 m and sound transmits through a temperature varying OML.

C. Dependence of Acoustic Propagation on Finescale Temperature Perturbations

The stated objective of this computer simulation has been to isolate all parameters affecting sound transmission to compare propagation through a real, temperature varying OML with propagation through a temperature invariant, idealized OML. Figure 8 through Fig 19 in Chapter IV indicate that acoustic transmission is markedly different through the two mixed layers. The spectra of acoustic fluctuations are impacted the most at frequencies above 2 kHz. The overall variance between the two cases at certain frequencies differs by as much as a factor of 5. However, temperature spectra do not modify either the average

acoustic pressure or the acoustic fluctuation spectra in a predictable pattern. Figure 23 shows average acoustic pressure, and Figure 24 shows variance of acoustic fluctuations plotted against frequency at each range analyzed. The data points marked 'x' are variance caused by propagation of a source at 35 m depth through a temperature varying environment. The data points marked 'o' are the same except transmission is through a temperature invariant OML. There is no clear trend. The probable cause of this is the strong dependence of sound on OML depth.

D. Dependence of Acoustic Propagation on Source Depth

To investigate depth dependence, the source depth of 35 m was modified at 3.5 kHz and at 5 kHz. The IFD-PE model simulated acoustic transmission through an idealized OML and a realistic OML at 3.5 kHz with source located at 5 m. Simulations were also run for a 5 kHz source located at 5 m, 30 m, and 45 m. The depth dependence of average acoustic pressure is shown in Fig 25, and the depth dependence of acoustic fluctuation variance is shown in Fig 26. Holding all parameters constant except depth can alter the variance of acoustic fluctuations by a factor of 5. Translating the sound source just 5 m from 35 m to 30 m increases acoustic fluctuations at 60 km in a temperature invariant OML three fold. This is evidence that the precise combination of source depth, frequency, and OML depth have a greater influence on acoustic transmission than does temperature perturbations. The source depth, frequency, and OML depth combination activate particular normal modes, which in turn raise and lower the average acoustic transmission and acoustic fluctuation density. This explains why temperature spectra do not modify the sound field in a predictable pattern. The realistic OML depth varies with range, changing which modes are activated. The change in geometry of the frequency wavelength compared to the source depth and OML depth with range is a stochastic process.

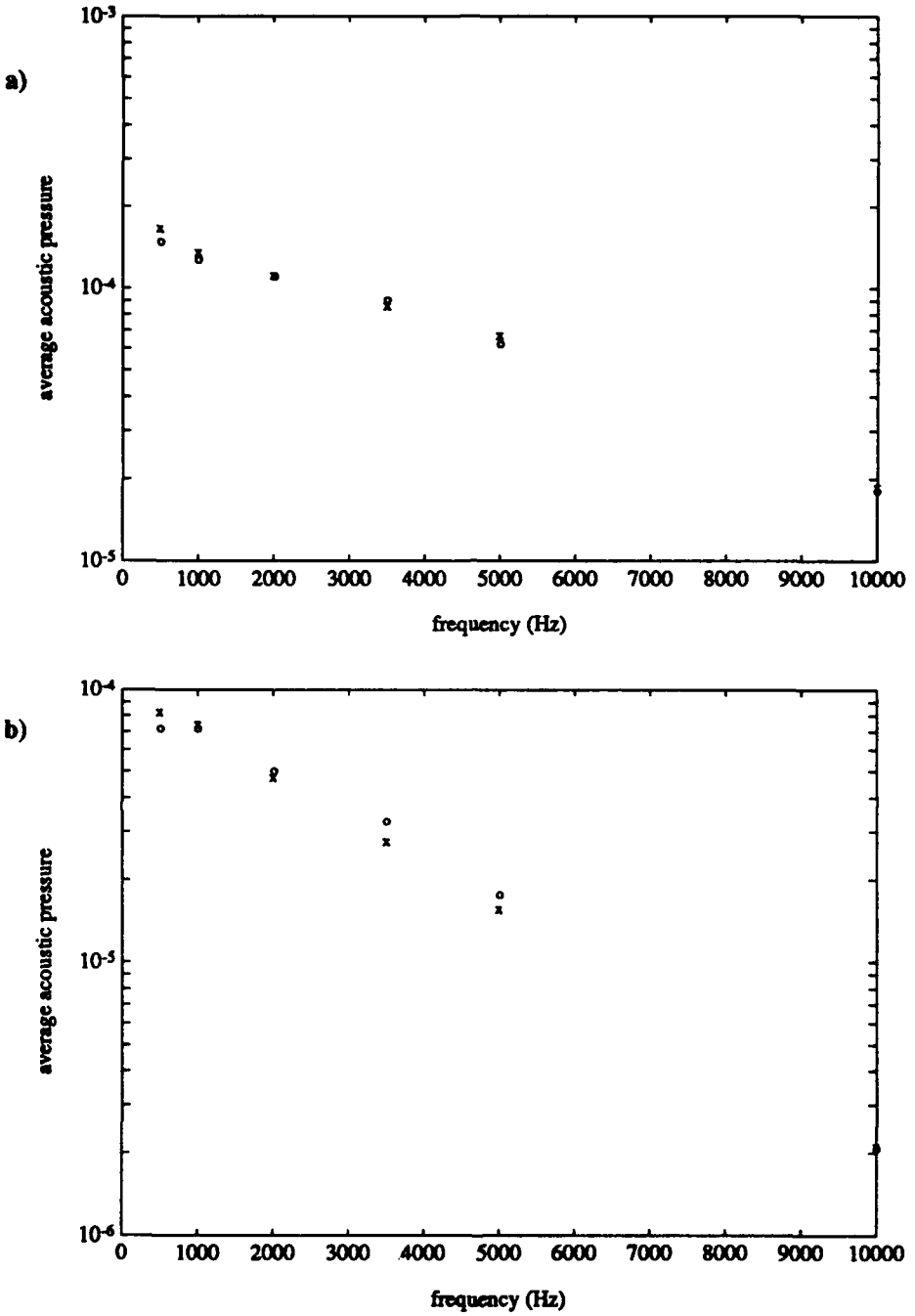

Fig 23. Depth averaged acoustic pressure as a function of frequency at range a) 20 km, b) 40 km. Source depth is 35 m. 'o' data points indicate results for the idealized OML. 'x' data points are for the temperature varying OML.

c)

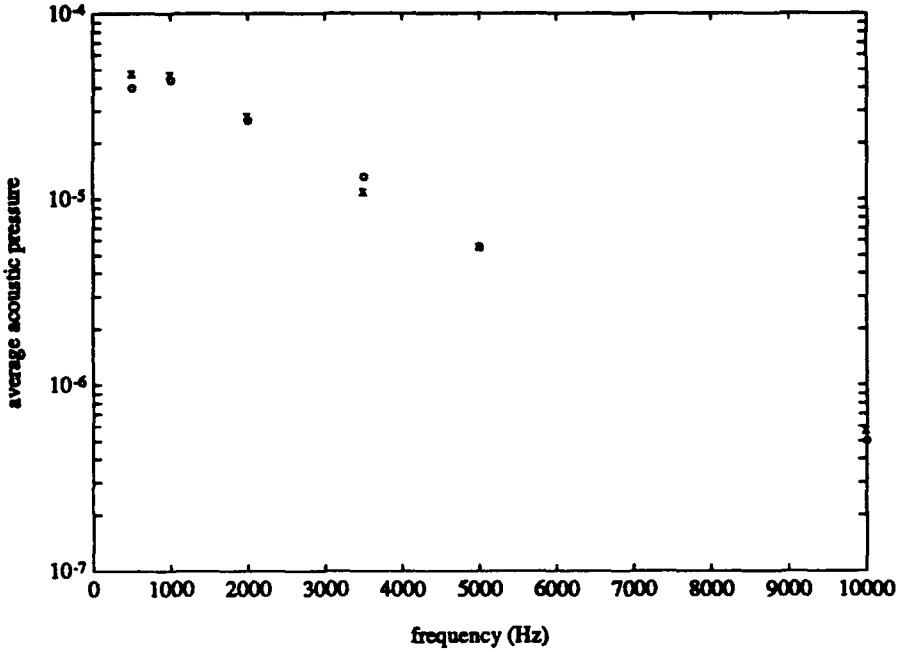

d)

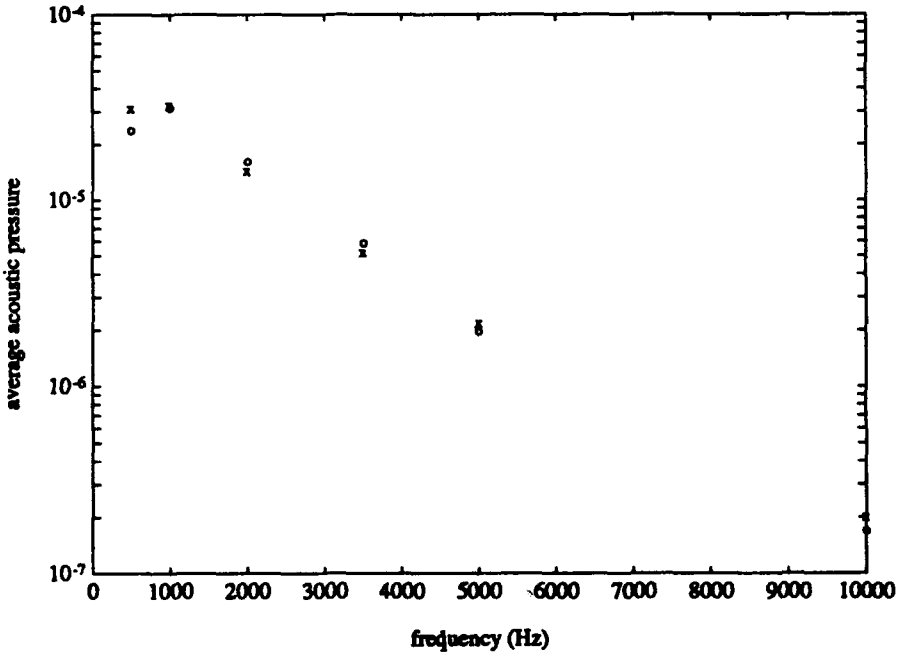

Fig 23. (cont) Depth averaged acoustic pressure as a function of frequency at range c) 60 km and d) 80 km. Source depth is 35 m. 'o' data points indicate results for the idealized OML. 'x' data points are for the temperature varying OML.

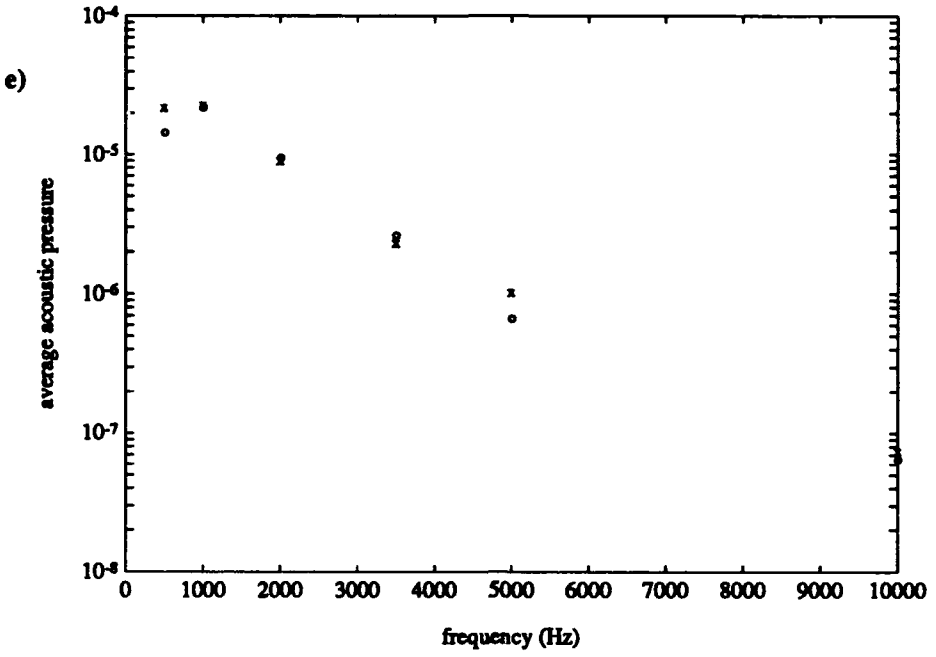

Fig 23. (cont) Depth averaged acoustic pressure as a function of frequency at range e) 100 km. Source depth is 35 m. 'o' data points indicate results for the idealized OML. 'x' data points are for the temperature varying OML.

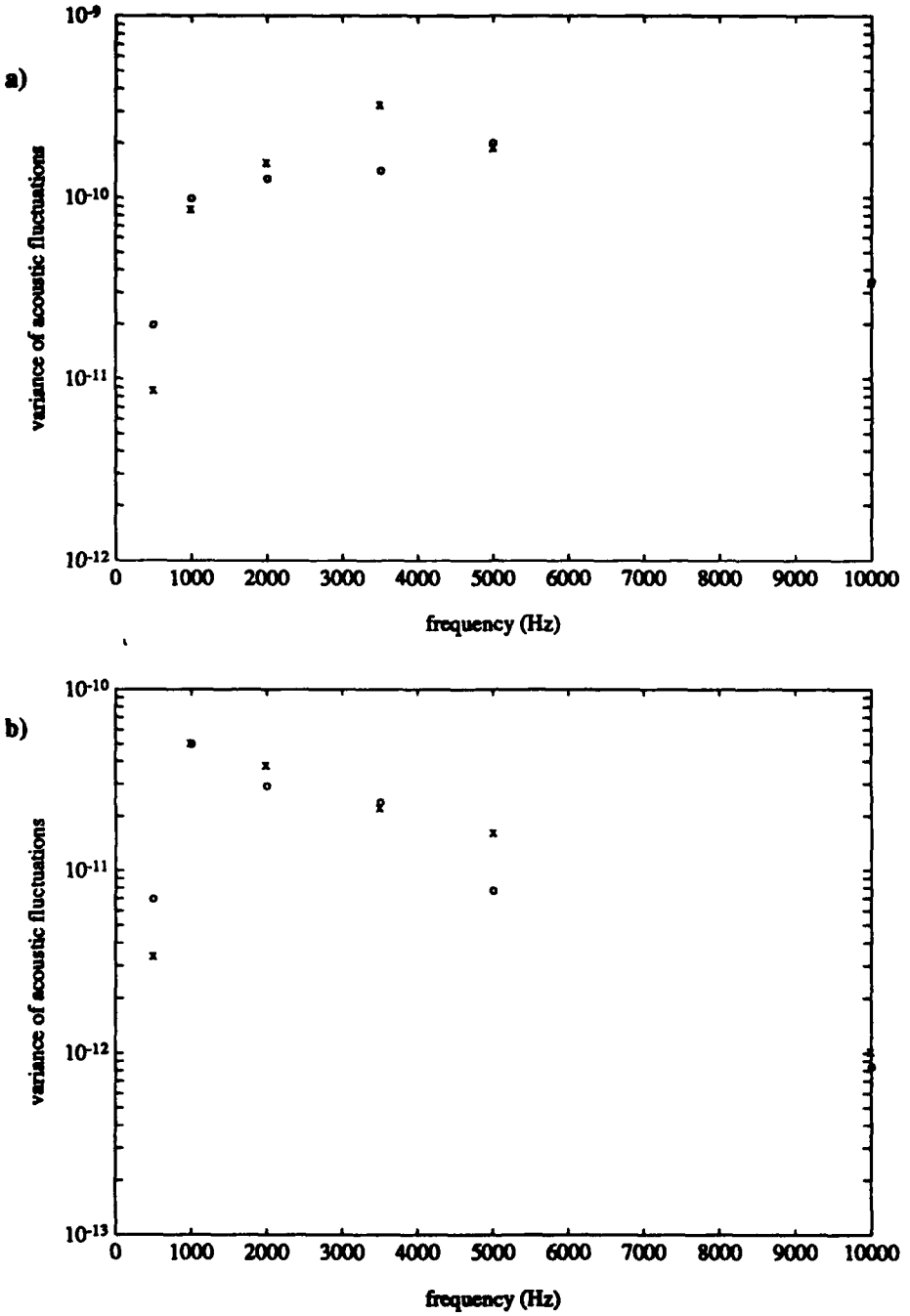

Fig 24. Variance of acoustic fluctuations as a function of frequency at range a) 20 km, b) 40 km. Source depth is 35 m. 'o' data points indicate results for the idealized OML. 'x' data points are for the temperature varying OML.

c)

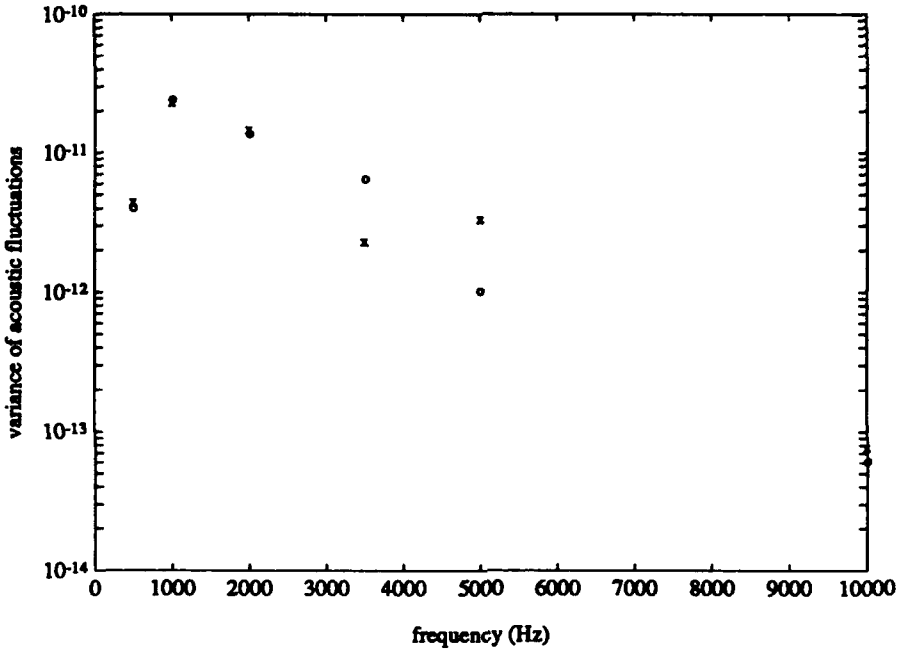

d)

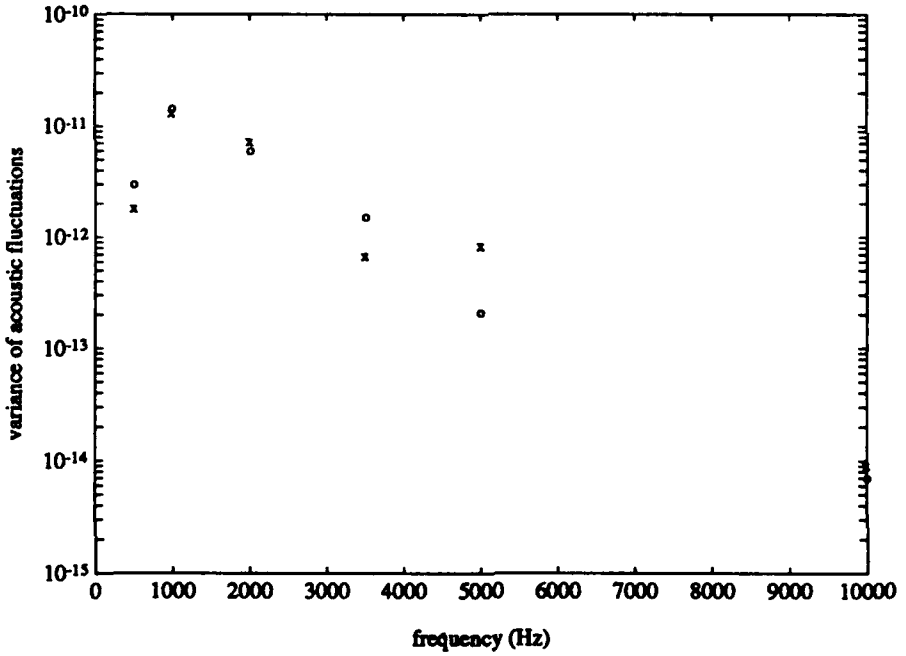

Fig 24. (cont) Variance of acoustic fluctuations as a function of frequency at range c) 60 km and d) 80 km. Source depth is 35 m. 'o' data points indicate results for the idealized OML. 'x' data points are for the temperature varying OML.

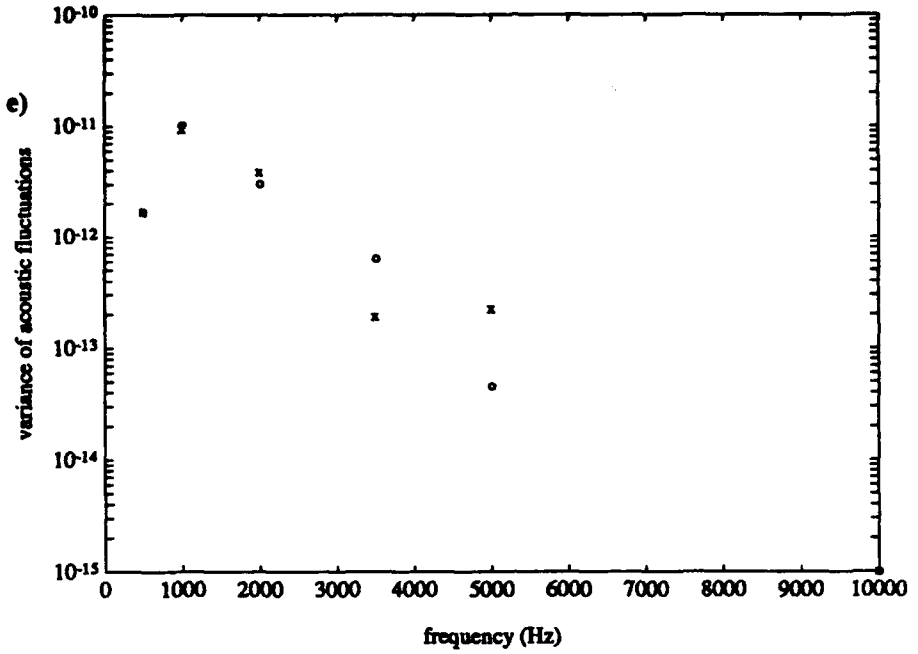

Fig 24. (cont) Variance of acoustic fluctuations as a function of frequency at range c) 60 km and d) 80 km. Source depth is 35 m. 'o' data points indicate results for the idealized OML. 'x' data points are for the temperature varying OML.

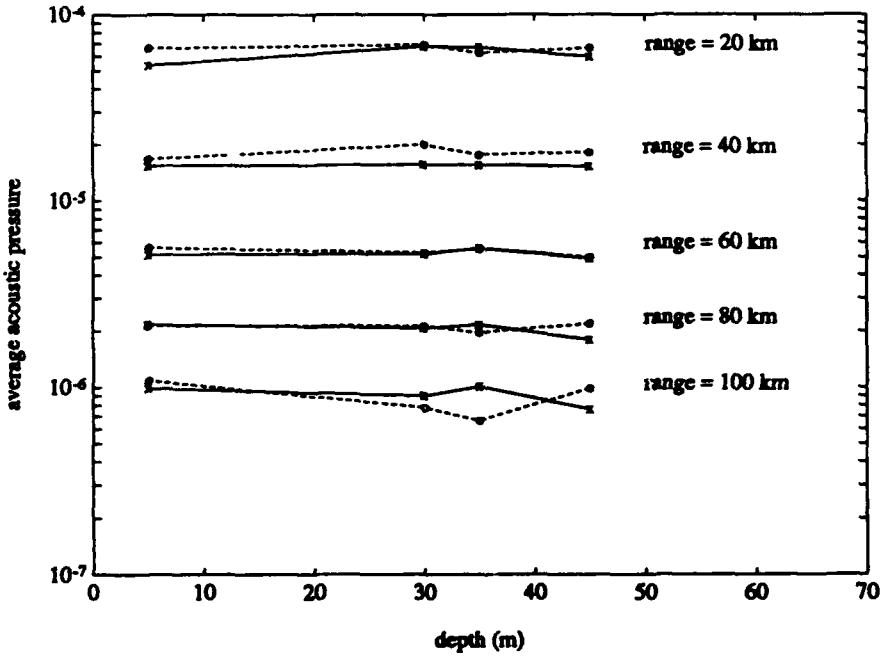

Fig 25. Dependence of average acoustic pressure on source depth for a 5 kHz source. 'x' indicates propagation through a temperature varying OML. 'o' indicates propagation through a temperature invariant OML.

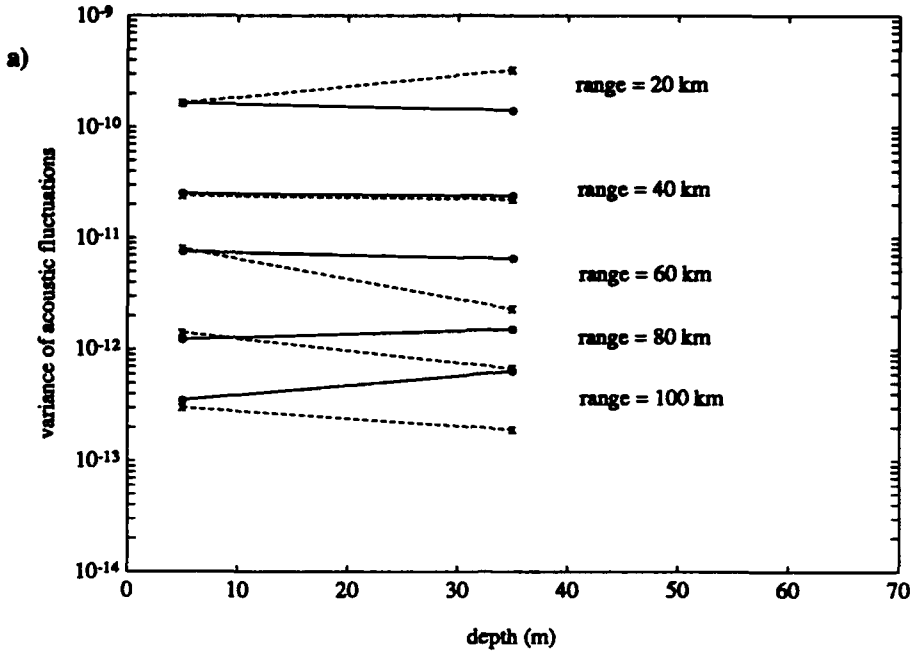

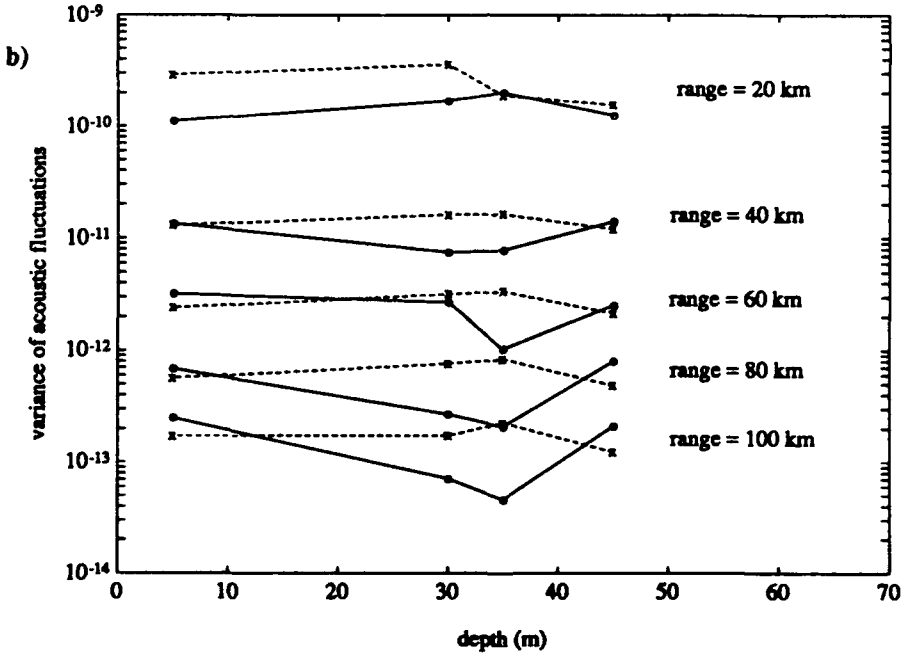

Fig 26. Dependence of variance of acoustic fluctuations on depth for a monofrequency source at a) 3.5 kHz, and b) 5 kHz. 'x' indicates propagation through a temperature varying OML. 'o' indicates propagation through a temperature invariant OML.

VI. CONCLUSIONS

A. HIGHLIGHTS

The IFD-PE model is a valuable tool to contrast acoustic transmission through a temperature varying OML with acoustic propagation through a temperature invariant OML. A computer experiment was designed using the transmission model that isolated all parameters capable of influencing sound propagation. A statistical analysis of the sound field enabled a direct comparison of the impact of temperature perturbations on acoustic propagation. Depth dependent average acoustic pressure was found to vary by up to a factor of two when contrasted for the two cases. Spatial variance of acoustic fluctuations was found to vary by up to a factor of five. Acoustic fluctuations are closely related to average sound pressure. The standard deviation of spatial fluctuations was found to be on the order of 10 percent of the depth averaged acoustic pressure. It is lower for low frequencies and much higher for high frequencies. Additional simulations with changes in source depth suggest that the impact of real temperature profiles on the sound field is indirect. It randomly modifies the normal modes that can propagate. This thesis proves that for medium acoustic frequencies propagating through a typical OML, an assumption of isothermal water and constant depth are valid.

B. SUGGESTIONS FOR FURTHER WORK

Additional effort is needed to verify the statistics of an ensonified surface duct. The approximate values of a factor of two for average acoustic pressure and ratio of one to ten for standard deviation to average acoustic pressure may be OML dependent. Also, no consideration was given to the horizontal dependence of temperature fluctuations. Each simulation started with the same sound velocity profile. If sound propagation is not modified by horizontal changes in source location, then temperature spectra alone are responsible for altering the sound field. If horizontal changes in source location alter the sound field, then precise temperature features are responsible.

LIST OF REFERENCES

Batchelor, G. K., et al, "Small-scale variation of convected quantities like temperature in turbulent fluid" (Parts 1 and 2), *J. Fluid Mech.*, 34, pp. 443-448, 1959.

Chernov, L. A., *Wave Propagation in a Random Medium* (translated by R. A. Silverman),: Dover Publications, New York, 1960.

Duda, T. F., et al, "Modelling meter-scale acoustic intensity fluctuations from oceanic fine structure and microstructure," *J. Geophysical Research*, 93, pp. 5130-5142, 1988.

Flatté, S. M. ed., *Sound Transmission Through a Fluctuating Ocean*, Cambridge University, New York, 1979.

Lee, D. and S. T. McDaniel, *Ocean Acoustic Propagation by Finite Difference Methods*, Pergamon Press, Oxford, 1987.

Mackenzie, K. V., "Equation of sound speed in the ocean," *J. acoust Soc. Am.*, 70, p. 808, 1981.

Medwin, H., *Predicting Sound Phase and Amplitude Fluctuations due to Microstructure in the Upper Ocean*, unpublished NPS technical report NPS-61Md73111A, 1973.

Neubert, J. A. and J. L. Lumley, "Derivation of the stochastic helmholtz equation for sound propagation in a turbulent fluid", *J. acoust Soc. Am.*, 48, pp. 1212-1218, 1970.

Tappert, F. D., "Parabolic equation method in underwater acoustics," *J. acoust. Soc. Am.*, 55, p. 534(A), 1974.

Tappert, F. D., "The parabolic equation method", *Wave propagation and Underwater Acoustics* (Eds. J. B. Keller and J. S. Papodakis); *Lecture Notes in Physics*, 70, Springer, Berlin, 1977.

Tatarskii, V. I., *The Effects of the Turbulent Atmosphere on Wave Propagation* (Israel Program for Scientific Translation), 1971.

Urick, R. J., "Measurements of the vertical coherence of the sound from a near-surface source in the sea and the effects on an additive vertical array," *J. acoust. Soc. Am.*, 54, pp. 115-120, 1973.

Urick, R. J, *Principles of Underwater Sound, 3rd Ed*, McGraw-Hill, New York, 1983.

Urick, R. J. and T. J. Tulko, "Vertical coherence of sound transmitted over a twenty four mile path," *J. Acoust. Soc. Am.*, 46, pp. 1308-1317, 1969.

INITIAL DISTRIBUTION LIST

Defense Technical Information Center Cameron Station Alexandria, VA 22304-6145	2
Dudley Knox Library Code 052 Naval Postgraduate School Monterey, CA 93943	2
Chairman, Code OC Oceanography Department Naval Postgraduate School Monterey, CA 93943	1
Assoc. Professor P.C. Chu Oceanography Department Naval Postgraduate School Monterey, CA 93943	1
Assoc. Professor A.A. Atchley Physics Department Naval Postgraduate School Monterey, CA 93943	1
Dr. J.C. Scott Admiralty Research Establishment Southwell, Portland Dorset DT5 2JS United Kingdom	1
Dr. D.S. Ko Institute for Naval Oceanography Stennis Space Center, MS 39529-5005	1
Oceanographer of the Navy Naval Observatory 34th and Massachusetts Avenue NW Washington, DC 20390-5000	1

Dr. D. Lee
Naval Underwater Systems Center
New London, CT 06320 1

Professor S.M. Flatté
Physics Department
University of California - Santa Cruz
Santa Cruz, CA 95064 1

Professor H. Medwin
Physics Department
Naval Postgraduate School
Monterey, CA 93943 1

CDR J. Fink
Commander Task Force Twelve
Pearl Harbor, HI 96601 1

LT G.D. Crabtree
Naval Air Facility ASWOC
Lajes Field, Azores 09720 1